



LUND UNIVERSITY

Chemical kinetics study of nitrogen-containing fuels in flames – experiments and modeling

Chen, Jundie

2025

Document Version:

Publisher's PDF, also known as Version of record

[Link to publication](#)

Citation for published version (APA):

Chen, J. (2025). *Chemical kinetics study of nitrogen-containing fuels in flames – experiments and modeling*. [Doctoral Thesis (compilation), Combustion Physics]. Department of Physics, Lund University.

Total number of authors:

1

General rights

Unless other specific re-use rights are stated the following general rights apply:

Copyright and moral rights for the publications made accessible in the public portal are retained by the authors and/or other copyright owners and it is a condition of accessing publications that users recognise and abide by the legal requirements associated with these rights.

- Users may download and print one copy of any publication from the public portal for the purpose of private study or research.
- You may not further distribute the material or use it for any profit-making activity or commercial gain
- You may freely distribute the URL identifying the publication in the public portal

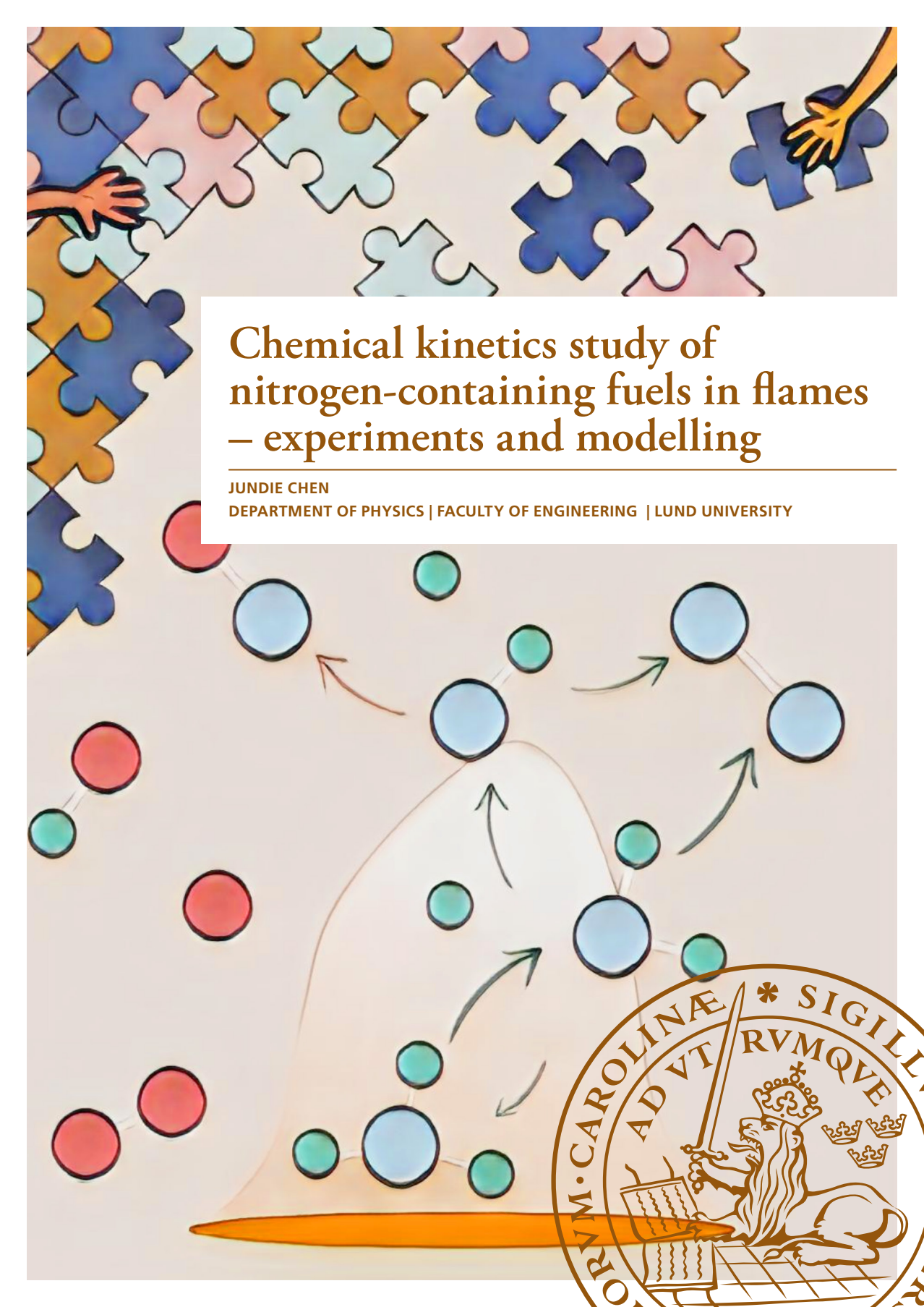
Read more about Creative commons licenses: <https://creativecommons.org/licenses/>

Take down policy

If you believe that this document breaches copyright please contact us providing details, and we will remove access to the work immediately and investigate your claim.

LUND UNIVERSITY

PO Box 117
221 00 Lund
+46 46-222 00 00



Chemical kinetics study of nitrogen-containing fuels in flames – experiments and modelling

JUNDIE CHEN

DEPARTMENT OF PHYSICS | FACULTY OF ENGINEERING | LUND UNIVERSITY





Chemical kinetics study of nitrogen-containing fuels in flames – experiments and modeling

Chemical kinetics study of nitrogen-containing fuels in flames – experiments and modeling

Jundie Chen



LUND
UNIVERSITY

DOCTORAL DISSERTATION

Doctoral dissertation for the degree of Doctor of Philosophy (PhD) at the Faculty of Engineering at Lund University to be publicly defended on 23rd of May 2025 at 13.15 in Rydbergsalen, Department of Physics, Professorsgatan 1

Faculty opponent

Prof. Christine Mounaïm-Rousselle
INSA-CVL, Université d'Orléans, Orléans, France

Organization: LUND UNIVERSITY

Document name: Doctoral dissertation

Date of issue: 2025-05-23

Author(s): Jundie Chen

Sponsoring organization:

Title and subtitle: Chemical kinetics study of nitrogen-containing fuels in flames – experiments and modeling

Abstract:

Climate change is strongly linked to the quantity of carbon dioxide (CO₂) released by burning fossil fuels, which contain carbon. To address the problem, ammonia (NH₃) has recently gained significant attention as a potential alternative fuel due to its carbon-free nature, ease of storage, and good energy density. However, ammonia combustion in practical devices presents challenges, particularly its high nitrogen oxides (NO_x) emissions and combustion behavior that differs significantly from conventional fuels.

Besides ammonia, nitrogen atoms are also commonly found in other fuels, such as coal, coal-derived oils, biomass, bio-oils, and wastes, predominantly incorporated in the form of pyrrolic and pyridinic heterocyclic functional groups. These nitrogen-containing compounds serve as precursors to fuel-NO_x during combustion.

Developing accurate chemical kinetic models is essential for understanding the reaction mechanisms of the combustion of nitrogen-containing fuels, as well as for predicting and optimizing fuel performance and reducing emissions. However, even for ammonia, a relatively light N-containing species, there is a lack of consensus regarding its reaction mechanisms and the associated kinetic parameters across existing models. To achieve a reliable and unified chemical kinetic model for these fuels, validations through fundamental combustion experiments are necessary. These experiments are specifically used to isolate and scrutinize detailed chemistry problems by minimizing the influence of complex flow and mixing effects. Besides, they provide valuable fundamental-level combustion data that characterizes the behavior of each fuel.

Therefore, this study conducted fundamental combustion experiments on nitrogen-containing fuels to provide two types of key fundamental combustion data—laminar burning velocity (LBV) and flame structure. LBVs were measured using the heat flux method, while flame structure was measured using a flat-flame configuration with the aid of Raman spectroscopy. In addition, related fundamental combustion data from the literature, obtained using methods such as spherical flame experiments, shock tubes, and flow reactors, were also used to support a more comprehensive model validation. All the modeling work was performed using ANSYS Chemkin-Pro software.

The research is based on five experimental and modeling studies, encompassing various fuel compositions, oxidizer environments, and temperature conditions. Each study explored a specifically designed fuel mixture aimed at addressing existing knowledge gaps. Variations in fuel composition alter the flame radical pool, allowing for the investigation of different chemical pathways within nitrogen combustion chemistry.

In the first study, pyrrole (C₄H₅N), the simplest five-membered nitrogen-containing aromatic molecule, was used as a model compound to investigate the fuel-bound nitrogen conversion mechanisms in the pyrrolic functional group. LBVs of pyrrole+air flames were measured, and the comprehensive kinetic model from our group was updated by incorporating reactions involving pyrrole and its intermediates.

Subsequent investigations focus on ammonia flames. Argon (Ar) was used as a diluent instead of conventional nitrogen (N₂) to elucidate specific ammonia flame chemistry. LBVs of ammonia+oxygen+argon mixtures were measured, and nine literature kinetic models were evaluated. The rate constants of three key reactions in ammonia chemistry were reviewed and updated in our model.

Further experiments were carried out to explore the LBVs of oxygen-enriched ammonia flames, which revealed discrepancies with previously reported LBV data, prompting model re-evaluations.

A separate study employs Raman spectroscopy for non-intrusive detection and quantification of nitric oxide (NO) and nitrous oxide (N₂O) in ammonia+oxygen+argon flames, providing valuable data for model validations.

Finally, ammonia was blended with nitromethane (CH₃NO₂), a precursor to NO, to elucidate the impact of NH₃–NO_x interactions. Interestingly, the results show that adding NH₃ has a non-monotonic effect on the LBV of the fuel blend, increasing the LBV only when the NH₃ fraction was below 70%. Kinetic analysis tools were used to explain this behavior, and our model was updated with a focus on CH₃NO₂ chemistry.

These findings collectively advance the understanding of the combustion characteristics of nitrogen-containing fuels and support the validation and refinement of existing chemical kinetic models.

Key words: Carbon-free; Ammonia; Nitrogen-containing fuels; Laminar burning velocity; Flame structure; Chemical kinetic models.

Classification system and/or index terms (if any)

Supplementary bibliographical information

Language: English

Number of pages: 195

ISSN: 1102-8718

ISBN: 978-91-8104-455-3 (print) 978-91-8104-456-0 (electronic)

Recipient's notes

Price

Security classification

I, the undersigned, being the copyright owner of the abstract of the above-mentioned dissertation, hereby grant to all reference sources permission to publish and disseminate the abstract of the above-mentioned dissertation.

Signature

Date 2025-04-08

Chemical kinetics study of nitrogen-containing fuels in flames – experiments and modeling

Jundie Chen



LUND
UNIVERSITY

Cover, front: Illustration of this thesis work by Jundie Chen, depicting a flat flame with simplified ammonia reaction paths and puzzle pieces being arranged by two hands, symbolizing collaboration in building chemical kinetic models. Designed in Canva with a cartoon-style effect applied using PortraitArt.

Cover, back: Photograph by Jundie Chen, taken during experimental work with ammonia.

Funding information: This thesis work is financially supported by the Knut and Alice Wallenberg (KAW) Foundation within the COCALD project.

Copyright pp 1–55 Jundie Chen

Paper I, II, & III © The authors

Paper IV & V © The authors (unpublished manuscript)

Faculty of Engineering

Department of Physics

ISBN: 978-91-8104-455-3 (print)

ISBN: 978-91-8104-456-0 (electronic)

ISSN: 1102-8718

LRCP: LRCP-268

ISRN: LUTFD2/TFCP-268-SE

Printed in Sweden by Media-Tryck, Lund University

Lund 2025



Media-Tryck is a Nordic Swan Ecolabel certified provider of printed material. Read more about our environmental work at www.mediatryck.lu.se

MADE IN SWEDEN 

知之为知之, 不知为不知, 是知也

Table of Contents

	Abstract	i
	Popular summary	iii
	Popular summary in Chinese.....	v
	List of papers.....	vii
	Related work	viii
	Paper summaries and author's contribution	x
	Abbreviations	xiii
1	Introduction	1
	1.1 The role of chemical kinetics.....	1
	1.2 Nitrogen-containing fuels	2
	1.3 Research questions and the thesis's scope.....	4
	1.4 Outline of the thesis.....	5
2	Concepts in chemical kinetics.....	7
	2.1 Chemical kinetics	7
	2.1.1 Global reaction and stoichiometry.....	7
	2.1.2 Elementary reactions and rate constant expressions.....	8
	2.2 Chemical kinetic model and determination of rate constants	12
	2.2.1 What is a chemical kinetic model?	12
	2.2.2 Determination of rate constants	14
	2.3 Chemical kinetic model validations	15
	2.3.1 Laminar flame experiments	16
	2.3.2 Other fundamental experiments.....	19
3	Experimental method - the heat flux method	21
	3.1 The apparatus.....	22
	3.2 Principle and LBV data processing method	25
	3.2.1 Principle.....	25
	3.2.2 LBV data processing method	27
	3.3 Uncertainty sources	30
	3.4 Flame instabilities and fuel corrosivity	31

3.4.1	Flame instabilities.....	31
3.4.2	Fuel corrosivity.....	33
4	Modeling method.....	34
4.1	Modeling for fundamental combustion experiments.....	34
4.1.1	Laminar burning velocity	34
4.1.2	Flame structure	35
4.1.3	Other experiments.....	36
4.2	Chemical kinetic analyses	37
4.2.1	A-factor sensitivity analysis	37
4.2.2	Rate of production analysis	38
4.2.3	Reaction pathway analysis.....	38
5	Results	39
5.1	Survey.....	39
5.2	NH ₃ +O ₂ +Ar mixtures	42
5.2.1	LBV results and modeling	42
5.2.2	Flame structure results and modeling.....	45
5.3	NH ₃ +O ₂ +N ₂ mixtures	46
5.4	CH ₃ NO ₂ +NH ₃ +air mixtures.....	48
6	Summary and outlook.....	52
6.1	Summary.....	52
6.2	Outlook.....	53
	Acknowledgements.....	54
	References	56

Abstract

Climate change is strongly linked to the quantity of carbon dioxide (CO_2) released by burning fossil fuels, which contain carbon. To address the problem, ammonia (NH_3) has recently gained significant attention as a potential alternative fuel due to its carbon-free nature, ease of storage, and good energy density. However, ammonia combustion in practical devices presents challenges, particularly its high nitrogen oxides (NO_x) emissions and combustion behavior that differs significantly from conventional fuels.

Besides ammonia, nitrogen atoms are also commonly found in other fuels, such as coal, coal-derived oils, biomass, bio-oils, and wastes, predominantly incorporated in the form of pyrrolic and pyridinic heterocyclic functional groups. These nitrogen-containing compounds serve as precursors to fuel- NO_x during combustion.

Developing accurate chemical kinetic models is essential for understanding the reaction mechanisms of the combustion of nitrogen-containing fuels, as well as for predicting and optimizing fuel performance and reducing emissions. However, even for ammonia, a relatively light N-containing species, there is a lack of consensus regarding its reaction mechanisms and the associated kinetic parameters across existing models. To achieve a reliable and unified chemical kinetic model for these fuels, validations through fundamental combustion experiments are necessary. These experiments are specifically used to isolate and scrutinize detailed chemistry problems by minimizing the influence of complex flow and mixing effects. Besides, they provide valuable fundamental-level combustion data that characterizes the behavior of each fuel.

Therefore, this study conducted fundamental combustion experiments on nitrogen-containing fuels to provide two types of key fundamental combustion data—laminar burning velocity (LBV) and flame structure. LBVs were measured using the heat flux method, while flame structure was measured using a flat-flame configuration with the aid of Raman spectroscopy. In addition, related fundamental combustion data from the literature, obtained using methods such as spherical flame experiments, shock tubes, and flow reactors, were also used to support a more comprehensive model validation. All the modeling work was performed using ANSYS Chemkin-Pro software.

The research is based on five experimental and modeling studies, encompassing various fuel compositions, oxidizer environments, and temperature conditions. Each study explored a specifically designed fuel mixture aimed at addressing existing knowledge gaps. Variations in the fuel compositions alter the flame radical pools, allowing for the investigation of different dominant chemistries within nitrogen combustion chemistry.

In the first study, pyrrole (C_4H_5N), the simplest five-membered nitrogen-containing aromatic molecule, was used as a model compound to investigate the fuel-bound nitrogen conversion mechanisms in the pyrrolic functional group. LBVs of pyrrole+air flames were measured, and the comprehensive kinetic model from our group was updated by incorporating reactions involving pyrrole and its intermediates.

Subsequent investigations focus on ammonia flames. Argon (Ar) was used as a diluent instead of conventional nitrogen (N_2) to elucidate specific ammonia flame chemistry. LBVs of ammonia+oxygen+argon mixtures were measured, and nine literature kinetic models were evaluated. The rate constants of three key reactions in ammonia chemistry were reviewed and updated in our model.

Further experiments were carried out to explore the LBVs of oxygen-enriched ammonia flames, which revealed discrepancies with previously reported LBV data, prompting model re-evaluations.

A separate study employs Raman spectroscopy for non-intrusive detection and quantification of nitric oxide (NO) and nitrous oxide (N_2O) in ammonia+oxygen+argon flames, providing valuable data for model validations.

Finally, ammonia was blended with nitromethane (CH_3NO_2), a precursor to NO, to elucidate the impact of NH_3 - NO_x interactions. Interestingly, the results show that adding NH_3 has a non-monotonic effect on the LBV of the fuel blend, increasing the LBV only when the NH_3 fraction was below 70%. Kinetic analysis tools were used to explain this behavior, and our model was updated with a focus on CH_3NO_2 chemistry.

These findings collectively advance the understanding of the combustion characteristics of nitrogen-containing fuels and support the validation and refinement of existing chemical kinetic models.

Popular summary

Solving a puzzle that shows the future!

Have you ever noticed some unusual fuel options at gas stations in Sweden, like liquefied biogas (labeled as LBG) and hydrogenated vegetable oil (labeled as HVO)? These are alternative fuels, representing a growing effort to combat climate change through cleaner energy sources. As we know, conventional fuels like gasoline and diesel release carbon dioxide (CO_2) when burned, a greenhouse gas contributing to global warming. In contrast, the biofuels mentioned above offer more environmentally friendly options.

But researchers are thinking beyond biofuels! They are exploring carbon-free fuel alternatives, such as hydrogen (H_2) and ammonia (NH_3). You might already be familiar with ammonia—it's used to produce fertilizers on the farm!

If you drive a gasoline-powered car, you might wonder: "Can I switch to a cleaner fuel and do my part for the environment?" Unfortunately, using alternative fuels isn't as simple as just refueling. In Sweden, LBG and HVO are primarily used in heavy-duty vehicles with modified engines. This is because alternative fuels have different combustion properties from conventional fuels, affecting their performance in existing engines.

Take gasoline as an example; let's do some quick math together on its burning velocity! Imagine you're driving in the city, and your dashboard shows the engine rotation speed is 2000 RPM (revolutions per minute). In a typical car, combustion happens once every two revolutions, meaning your engine experiences 1000 combustion cycles per minute—or about 17 cycles per second. Each combustion cycle lasts roughly 0.06 seconds ($1/17$), with about a quarter of that time—0.015 seconds—dedicated to actual flame propagation. Assume a cylinder diameter of 8 cm, then the flame must at least travel at a speed of $4/0.015 \approx 266$ cm/s from the center of the spark plug to the wall! Not all fuels can meet this requirement. Ammonia, for instance, burns at less than half the speed of gasoline. Therefore, researchers suggest that ammonia must be blended with other active fuels or used in applications where fast combustion isn't crucial, such as ships.

The above situation raises an important question: Can we use simulations to predict how fuels behave? If so, engineers could strategically modify and optimize the combustion before using them in reality!

This is where my research comes into play!

Since combustion is a sequence of chemical reactions between fuel and oxidizer, if we can accurately describe all the chemical reactions and their reaction rates during combustion, we will have grasped the core mechanism of combustion. By further

integrating physical models of the flow and heat transfer, we can achieve a comprehensive understanding of the combustion process!

Therefore, our research group developed a combustion chemistry model to map the reactions occurring during fuel combustion. Our models predict how and how fast fuel molecules break down, form new compounds, and react with each other under different conditions.

Building a combustion chemistry model for a specific fuel is like solving a giant puzzle:

- ✚ Each chemical species that might appear during combustion is a puzzle piece; if you're missing pieces, you can't see the whole picture!
- ✚ The connection between each puzzle piece is the reaction path. You must also place the pieces correctly to make the puzzle look good.
- ✚ When you solve a puzzle, you might start with the edge pieces and fill in the inner pieces to make it easier since they have fewer connections with other pieces and can be put in the correct positions more quickly. When we build up the model, we also always start with the species that are easier to be isolated from other species, i.e., they have fewer interaction reactions with other species. To do this, we design and conduct experiments that could isolate specific species and their reactions for investigation. You can check out my thesis to know how I do that!

For my Ph.D. research, I focus on solving the combustion chemistry puzzle of ammonia. Ultimately, our goal is to solve a giant puzzle that includes a lot of alternative fuels! Thus, we can see their combustion picture — a more sustainable and clean future!

Popular summary in Chinese

科普简介: 拼图游戏, 拼出“未来”!

在瑞典, 你可能会在加油站见到一些颇具特色的燃料, 比如液化生物天然气 (LBG) 和加氢植物油 (HVO)。它们属于目前备受关注的清洁燃料之一。大家都知道, 我们日常使用的汽油和柴油属于传统的化石燃料, 在燃烧过程中会释放大量二氧化碳(CO_2), 这是导致全球变暖的主要原因之一。而相比之下, 这两种生物燃料不仅排放的 CO_2 更少, 它们的原料来源也更加可持续。

事实上, 除了生物燃料, 科研人员还在积极探索一些零碳燃料, 比如氢气 (H_2) 和氨 (NH_3)。你可能对氨并不陌生——它常被用作农场化肥的主要原料!

你可能会问: “我也想为环保出一份力, 那我能不能直接改用这些清洁燃料呢?”。可惜, 事情并没有那么简单。以瑞典为例, 前面提到的 LBG 和 HVO 目前几乎只应用于经过特殊改装的重型车辆, 比如卡车。更换成替代燃料并不像加油那么轻松, 毕竟, 不同燃料的“脾气”各不相同, 烧起来的方式也各有讲究, 不能一概而论。

举个例子, 让我们来看看汽油到底烧得有多快吧! 假设你正在开一辆普通小汽车, 仪表盘显示发动机转速是 2000 转/分钟。对普通发动机, 每两次转动才发生一次燃烧, 这就意味着发动机每分钟经历 1000 次燃烧循环。换算到每秒钟的话, 大约每秒 17 次燃烧循环。那么每次燃烧循环持续 $1/17 \approx 0.06$ 秒, 其中只有约 $1/4$ 的时间是用于火焰传播的, 那就是 $0.06/4=0.015$ 秒。如果气缸直径为 8 cm, 则火焰传播速度需要达到至少 $4/0.015 \approx 266$ cm/s 才能从气缸中心传播到气缸壁面! 但问题来了: 不是所有燃料的火焰都能跑这么快。比如氨, 它的燃烧速度不及汽油的一半。因此科学家们通常建议要么把氨跟一些活跃的燃料混合使用; 要么把它安排到对燃烧速度要求不那么高的场景中, 比如船上。

上面这个例子引出了一个很自然的问题: 我们能不能直接用计算机来模拟燃烧过程, 提前预测这些新型燃料的表现呢? 想想看, 如果真的能做到这一点, 那么在实际使用以前, 我们就能大致判断出“这个燃料到底该怎么烧才最合适”!

这正是我的博士课题大显身手的地方!

燃烧本质上是一系列燃料与氧化剂的化学反应过程: 如果我们能描述出燃烧中所有发生的化学反应和反应的快慢, 那么我们就掌握了燃烧的核心! 再结合物理层面的流动、换热, 我们就能全面解析燃烧!

因此，我的研究团队致力于开发和优化各种燃料的燃烧化学模型，用于描述燃料分解、中间物种的生成、物种之间的反应的详细过程，及其在不同温度和压力下的反应速率。

构建一个燃料的燃烧化学模型，就像完成一幅大型拼图：

- ✚ 燃料燃烧时涉及的每种化学物质，就像拼图中的一个碎片，如果缺少某些碎片，就无法还原完整的拼图！
- ✚ 拼图碎片之间的连接关系就是反应路径——必须正确排列，才能得到最终合理的拼图。
- ✚ 拼图时，我们通常会先拼边缘，再填充中间部分，因为边缘碎片连接更少，更容易找到正确位置。同样，在研究燃烧化学模型时，我们优先研究那些与其他物质反应较少的化学物种，然后再逐步推导，填补其余连接部分。为了分离出这些物种和它们的反应，我还会设计、进行实验。如果你感兴趣，可以查看我的论文，看我是如何做到的！

在我的博士研究中，我专注于破解氨燃烧的“拼图”。我们的最终目标是破解一张覆盖多种清洁燃料的大型“燃烧全图”。等拼图完成的那一天，我们就能清楚地“看见”它们燃烧的模样！

List of papers

This thesis is based on the following papers:

Paper I :

M. Lubrano Lavadera, **J. Chen**, A.A. Konnov, Laminar burning velocities of pyrrole/air flames: Experimental and comprehensive modeling study, Combustion and Flame 245 (2022) 112350.

Paper II:

J. Chen, M. Lubrano Lavadera, A.A. Konnov, An experimental and modeling study on the laminar burning velocities of ammonia+oxygen+argon mixtures, Combustion and Flame 255 (2023) 112930.

Paper III:

J. Chen, X. Han, A.A. Konnov, Data consistency of the laminar burning velocity of oxygen-enriched $\text{NH}_3 + \text{O}_2 + \text{N}_2$ mixtures and kinetic modeling, Fuel 385 (2025): 134017.

Paper IV:

A. Zubairova, **J. Chen**, A.A. Konnov, C. Brackmann. Flame structure study of premixed $\text{NH}_3/\text{O}_2/\text{Ar}$ flames using Raman spectroscopy, Combustion and Flame (under revision).

Paper V:

J. Chen, A.A. Konnov. When ammonia addition increases the burning velocity of a fuel blend, Combustion and Flame (under revision).

Related work

The following papers are related works but not included in the thesis:

Paper I:

A.A. Konnov, **J. Chen**, M. Lubrano Lavadera, Measurements of the laminar burning velocities of 1,2-butadiene: A comparative study, Proceedings of the Combustion Institute 40 (2024) 105573.

Paper II:

A.A. Konnov, **J. Chen**, M. Lubrano Lavadera, Measurements of the laminar burning velocities of small alkyl esters using the heat flux method: A comparative study, Combustion and Flame 255 (2023) 112922.

Paper III:

A.A. Konnov, **J. Chen**, M.L. Lavadera, Laminar burning velocities of cyclopropane flames, Combustion and Flame 246 (2022) 112395.

Paper IV:

Q. Lin, X. Hu, **J. Chen**, A.A. Konnov, Measurements of laminar burning velocities and an improved kinetic model of methyl isopropyl ketone, Combustion and Flame 258 (2023) 113041.

Paper V:

Q. Lin, **J. Chen**, X. Hu, C. Zou, A.A. Konnov, Measurements of laminar burning velocities and kinetic modeling of two symmetrical ketones: di-ethyl ketone and di-isopropyl ketone, Combustion and Flame 268 (2024) 113614.

Paper VI:

X. Hu, **J. Chen**, Q. Lin, A.A. Konnov, Experimental and kinetic modeling study of the laminar burning velocity of CH_4/H_2 mixtures under oxy-fuel conditions, Fuel 376 (2024) 132597.

Paper VII

X. Hu, **J. Chen**, Q. Lin, A.A. Konnov, Effects of elevated oxygen content and temperature on the laminar burning velocity of the blast furnace gas in oxygen-enriched air condition, Fuel 380 (2025) 133114.

Paper summaries and author's contribution

Paper I : Laminar burning velocities of pyrrole/air flames: Experimental and comprehensive modeling study.

M. Lubrano Lavadera, J. Chen, A.A. Konnov (2022).

Laminar burning velocities for pyrrole/air flames were determined over equivalence ratios ranging from 0.6 to 1.3, at 338 K and 1 atm. The detailed kinetic model of the authors was extended by the reactions of pyrrole and its intermediates based on previous theoretical studies and analogies to reactions of similar species. Modifying the rate constant of the reaction, $C_4H_5N+OH=H_2O+PYRLYL$ was suggested, dramatically improving the model performance. The model was also validated for literature laminar burning velocities, speciation data in reactors, and ignition delay times in shock tubes of various pyrrole mixtures and showed overall good performances.

Dr. M. Lubrano Lavadera and I carried out the experiments. I conducted model simulations, and Prof. A.A. Konnov improved the kinetic model. Dr. M. Lubrano Lavadera wrote the manuscript, and all authors contributed to editing.

Paper II: An experimental and modeling study on the laminar burning velocities of ammonia+oxygen+argon mixtures.

J. Chen, M. Lubrano Lavadera, A.A. Konnov (2023)

The laminar burning velocity of ammonia was measured in mixtures diluted with argon using the heat flux method at an initial temperature of 298 K and atmospheric pressure over an equivalence ratio range of 0.4–1.5. Nine recent ammonia kinetic models were selected and validated against these new experimental data. The model from our group was revisited, and the rate constants for three reactions, $NH_2+H(+M)=NH_3(+M)$, $NNH+O=NH+NO$, and $NH_2+O=HNO+H$ were updated.

I carried out experiments, simulations, and kinetic model improvements. Prof. A.A. Konnov contributed to conceptualization and the kinetic model improvements. I was responsible for preparing the manuscript, which all authors contributed to.

Paper III: Data consistency of the laminar burning velocity of oxygen-enriched $NH_3+O_2+N_2$ mixtures and kinetic modeling.

J. Chen, X. Han, A.A. Konnov (2025)

Laminar burning velocities of ammonia in oxygen-enriched air (oxygen content ranging from 30 to 50 vol.%) were investigated under various initial temperatures (298, 323, and 348 K) at a pressure of 1 atm. The measurements revealed substantial

disparities with previously published data, and the discrepancies were analyzed. The model from our research group was modified by revisiting the rate constants, particularly in the context of N_2H_2 and NH_2O reactions, and third body collisional efficiencies of NH_3 following recent theoretical studies, led to improved predictions for the LBV in present flames, NH_3+H_2 +air flames, and NH_3 +air flames at elevated temperatures.

I carried out experiments, simulations, and kinetic analyses. Dr. X. Han contributed to experimental data validations. Prof. A.A. Konnov carried out the kinetic model improvements. I was responsible for preparing the original manuscript, Prof. A.A. Konnov was responsible for writing the kinetic modeling part and editing the manuscript, and Dr. X. Han contributed to editing the manuscript.

Paper IV: Flame structure study of premixed $\text{NH}_3/\text{O}_2/\text{Ar}$ flames using Raman spectroscopy.

A. Zubairova, **J. Chen**, A.A. Konnov, C. Brackmann (under revision).

Raman spectroscopy was employed with multiple laser beam passages to carry out non-intrusive detection and quantification of two NO_x species, NO and N_2O , in $\text{NH}_3+\text{O}_2+\text{Ar}$ flames with detection limits of 600 and 250 ppm, respectively. The processed datasets were then compared with predictions of four chemical kinetic mechanisms, and possible reasons for disagreements in their predictions were suggested. The model from our group was updated by implementing rate constants results, especially for the N_2O species.

My colleague A. Zubairova carried out Raman spectroscopy measurements and data analysis and wrote the original manuscript; I carried out the simulations, kinetic analyses, visualization of the experimental data and modeling results, and corresponding writing. Dr. Christian Brackman contributed to the methodology, Prof. A.A. Konnov contributed to the kinetic modeling, and Dr. Christian Brackman and Prof. A.A. Konnov contributed to the conceptualization, review, and editing together.

Paper V: When ammonia addition increases the burning velocity of a fuel blend.

J. Chen, A.A. Konnov. (under revision)

Ammonia was blended with nitromethane (CH_3NO_2), which was used as a nitric oxide (NO) precursor. The laminar burning velocities (LBV) of $(\text{CH}_3\text{NO}_2+\text{NH}_3)$ +air mixtures were investigated across a wide range of NH_3 mole fractions in the fuel blends, from 0% to 80%, spanning fuel-lean to fuel-rich conditions, at an initial temperature of 338 K and 1 atm. The results show that adding NH_3 enhances the

reactivity of CH_3NO_2 when the NH_3 fraction in the fuel is below 70%. The kinetic model from our group was updated, primarily on CH_3NO_2 chemistry, and shows very good agreement with the measurements without any rate constants tuning. Detailed kinetic analyses based on the present model reveal that the reaction $\text{NH}_2 + \text{NO} = \text{NNH} + \text{OH}$ significantly impacts the LBV even when a small portion of NH_3 is added to the fuel blend. NH_3 addition is found to increase adiabatic flame temperature and enrich the active radical pool of H, OH, and O as well.

I carried out experiments, simulations, and kinetic analyses. Prof. A.A. Konnov contributed to conceptualizing and carrying out the model improvements. I was responsible for preparing the original manuscript. Prof. A.A. Konnov prepared the writing of the kinetic modeling part and contributed to the review and editing.

Abbreviations

CFD	Computational fluid dynamics
C.E.M.	Controlled evaporator and mixer
Cori-Flow MFC	Coriolis mass flow controller
GHG	Greenhouse gas
HAB	Height above the burner surface
HHV	Higher heating value
IDT	Ignition delay time
JSR	Jet-stirred reactor
LBV	Laminar burning velocity
LHV	Lower heating value
MFC	Mass flow controller
PFR	Plug flow reactor
RCM	Rapid compression machine
ROP	Rate of production
ST	Shock tube

1 Introduction

1.1 The role of chemical kinetics

Combustion is one of the primary approaches to acquire and utilize energy for human activities, from transportation to electricity generation, affecting every aspect of life. Understanding combustion requires multidisciplinary knowledge spanning chemistry, physics, fluid dynamics, thermodynamics, mathematics, and computer science [1]

At the core of combustion science lies chemical kinetics, which governs the rates of chemical reactions occurring during the combustion process. As Nobel laureate Nikolay Semenov stated in his 1956 lecture, every combustion process *“is above all a chemical reaction between the components of the combustible mixture, accompanied by the liberation of heat and various kinds of motion in gases. For this reason, all phenomena which occur in the combustion process are closely linked with the ideas and laws of chemical kinetics.”*

Figure 1.1, adopted from Curran [1], illustrates the steps to understand the combustion and application of a fuel, clearly emphasizing the central role of chemical kinetics in modern combustion science. In this figure, a chemical kinetic model encompassing chemical kinetics, thermodynamics, and transport properties of species, describes fuel combustion at a molecular level and is indispensable to achieve low-emission and high-efficiency combustion. Building such a model requires theoretical calculations, experimental validation, and iterative refinement. Once obtained, the models can be reduced and integrated with physical sub-models of turbulence, mixing, and heat transfer to be applied in computational fluid dynamics (CFD) simulations, which are then combined with laboratory-scale combustion tests to aid in the design of combustors.

This study focuses on conducting fundamental experiments to validate and refine the gas-phase chemical kinetics within detailed models, as indicated by the blue text in Figure 1.1, with a particular emphasis on nitrogen-containing fuels. The primary laboratory technique employed in this work is the heat flux method, which is used to obtain laminar burning velocity (LBV) data.

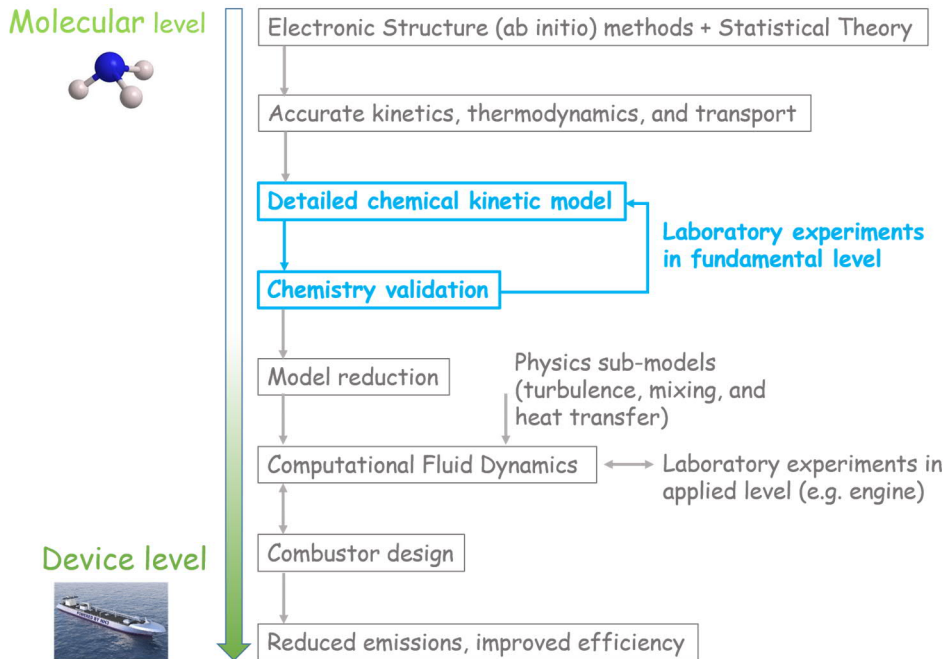


Figure 1.1 Schematic diagram illustrating the steps to understand the combustion and application of a fuel. Recreated from Curran [1].

1.2 Nitrogen-containing fuels

Following the Paris Agreement on climate change in 2015 [2], the global combustion community has placed a stricter emphasis on reducing greenhouse gas (GHG) emissions. Combustion of conventional hydrocarbon fuels, such as coal and oil, produces carbon dioxide (CO_2), a major greenhouse gas contributing to environmental and human health concerns. According to the Emissions Database for Global Atmospheric Research (EDGAR) [3], till the year 2023, fossil CO_2 accounted for 73.7% of total GHG emissions, followed by CH_4 (18.9%) and N_2O (4.7%).

To meet global decarbonization goals, it is essential to replace a significant percentage of fossil fuels with renewable energy sources. However, energy production from most renewable energy sources, such as wind, wave, tidal, and solar are inherently intermittent. Various energy storage solutions are available to cushion the effects of fluctuation in energy production, such as batteries for direct electricity

storage or pumped-storage hydropower to produce electricity on demand. Chemical energy storage appears to be the only sufficiently flexible mechanism allowing large quantities of energy to be stored over long time periods at any location [4].

In this context, ammonia (NH_3) has gained significant attention as a potential energy carrier, largely due to the established interest in the envisioned “hydrogen economy” [5]. While hydrogen (H_2) is an attractive energy carrier due to its high mass energy content and Lower Heating Value (LHV), it faces challenges in terms of economical storage and transportation, along with safety risks due to its extremely high reactivity [6, 7]. A practical solution to these drawbacks can be found by converting H_2 into a carbon-free, hydrogen-carrying fuel such as ammonia (NH_3) via a well-established industrial process [4, 7-10]. Ammonia is one of the most synthesized chemicals globally. It can be stored in liquid form under moderate pressure (10 bar) at ambient temperatures (25°C), offering higher volumetric hydrogen density than liquid hydrogen itself [4, 7-10] while reducing storage costs by 26–30 times compared to hydrogen [11]. As a result, many countries have designated ammonia as a “hydrogen carrier” [4, 6-11].

The option of directly using ammonia as a fuel was also considered since converting ammonia back to hydrogen would increase the cost and energy spent, although it is possible. Ammonia exhibits good energy density [4, 9], as shown in Figure 1.2, the volumetric energy density of liquid ammonia is higher than that of liquid hydrogen and some batteries, which is one of the qualities that make it attractive for energy storage and transport. However, integrating ammonia into combustion applications presents several challenges due to its low flammability and high autoignition temperature [4, 9], making it difficult to ignite and sustain combustion. Ammonia combustion produces a significant amount of nitrogen oxides (NO_x) and might produce nitrous oxide (N_2O) and unburned NH_3 , depending on the combustion conditions [12-14], all of which are harmful pollutants.

Despite these challenges, ammonia remains a highly active research topic, and extensive studies on its combustion have been carried out in recent years, as summarized in the reviews [4, 9, 15, 16]. Strategies currently under discussion to improve the combustion performance of ammonia include co-firing ammonia with reactive fuels in engines [17-20] or applying ammonia in combustors that do not require high combustion intensity, such as in gas turbines and marine engines [21-23].

Beyond its role as a fuel, ammonia is also an impurity commonly found in gaseous fuels derived from gasification processes of biomass or coal and is one of the largest sources of nitrogen contributing to nitrogen oxide (NO) formation during coal combustion [12]. Therefore, understanding the combustion chemistry of ammonia is crucial, both for integrating ammonia as a fuel in combustion systems and for understanding the mechanisms of fuel- NO_x formation and mitigation. Ammonia, a

relatively simple nitrogen-containing species, also serves as a good model for nitrogen-containing fuels' combustion chemistry investigations.

Additionally, other nitrogen-containing species are also prevalent in alternative and conventional fuels. For example, nitrogen in coal, coal-derived oils, biomass, bio-oils, and wastes is predominantly incorporated in the form of pyrrolic and pyridinic heterocyclic functional groups, which are precursors of fuel-NO_x in the combustion. Therefore, this study also investigated pyrrole (C₄H₅N), the simplest five-membered nitrogenous aromatic molecule, as a model compound to study the conversion mechanisms of fuel-bound nitrogen in the pyrrolic functional groups.

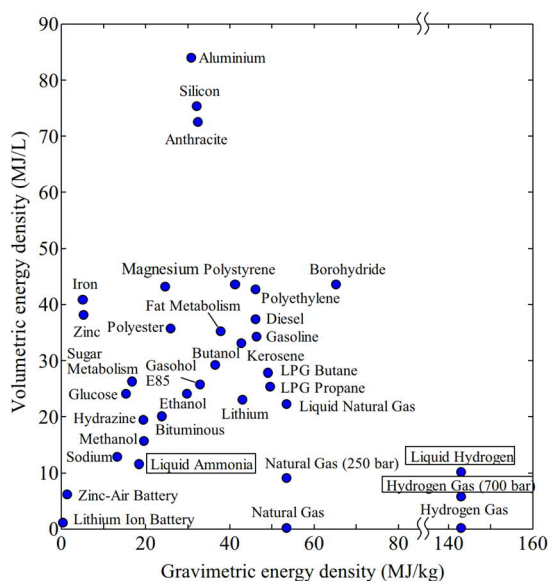


Figure 1.2 Gravimetric and volumetric energy density of combustible materials and batteries. Higher heat value (HHV) for fuels are used. Reproduced from [9].

1.3 Research questions and the thesis's scope

Even though ammonia is a light nitrogen-containing compound, its combustion chemistry is still not very well known. This is illustrated by the flurry of experimental and modeling work in recent years, as summarized in [24, 25]. More significant efforts are still needed to improve the accuracy of ammonia chemical

kinetic models and expand to other larger fuel-derived nitrogen-containing species. In a 2022 review regarding the prospects and challenges of ammonia as a fuel, Herbinet et al. [16] posed a key question: can we develop a unified kinetic model for ammonia combustion? They noted that a major obstacle is the lack of consensus on kinetic parameters within existing chemical kinetic models, stating: *“This problem is not insoluble, but it takes time and effort to find a general agreement on the best set of kinetic parameters to be used and the release of a quasi-unified model. This quest is still far from conclusion for ammonia”*. Similarly, Alturaifi et al. [26] highlighted the difficulty of selecting a reliable ammonia kinetic model, remarking: *“There are few, if any, other molecules for which such a large number of detailed kinetic models have been proposed within the past 5–6 years. Picking what seems to be the best detailed kinetic model to design a combustion device running on NH₃ could be a difficult task to start with”*.

There is a clear need to assess existing kinetic models, propose new experiments, and develop further validated models, focusing on the NH₃ chemistry and extending to other important fuel-derived nitrogen-containing species. Therefore, this research is based on a series of experimental and modeling studies, covering a range of fuel compositions, oxidizer environments, and temperature conditions. Each study investigated designed fuel mixtures, specifically selected to address existing knowledge gaps in nitrogen combustion chemistry.

In Paper *I*, laminar burning velocities of pyrrole+air flames were investigated. The kinetic model from our group was updated with a focus on pyrrole chemistry.

In Paper *II*, laminar burning velocities of ammonia+oxygen+argon flames were studied, supporting the validation and refinement of ammonia chemistry in the kinetic model.

In Paper *III*, discrepancies in the laminar burning velocities of oxygen-enriched ammonia flames within literature were analyzed, and further revisions were made to the rate constants in ammonia chemistry.

In Paper *IV*, Raman spectroscopy was used to quantify NO and N₂O profiles in ammonia flames, results were compared with various literature models, and the N₂O chemistry in our model was refined.

In Paper *V*, ammonia was blended with nitromethane (CH₃NO₂), and laminar burning velocities were measured across a range of blending ratios. The kinetic model was further updated by adding CH₃NO₂ chemistry.

1.4 Outline of the thesis

The thesis is structured as follows:

Chapter 2 introduces key concepts in chemical kinetics relevant to this study, explains what a chemical kinetic model is, and discusses typical fundamental combustion experiments used for model validation.

Chapter 3 outlines the experimental method, the heat flux method, employed for laminar burning velocity measurements

Chapter 4 describes the modeling approaches used in this work, including methods for simulating fundamental combustion experiments and tools for chemical kinetic analysis.

Chapter 5 presents the main research findings.

Chapter 6 provides a summary of the study and discusses future research directions.

2 Concepts in chemical kinetics

2.1 Chemical kinetics

The study of chemical kinetics involves understanding the transition process from reactants to products, and answers the questions of “why” and “how” reactions occur [27]. As shown in Figure 2.1, for a reaction $A \rightarrow B$, chemical kinetics describes the evolution of the system over time, while thermodynamics predicts the chemical equilibrium state, when time approaches infinity.

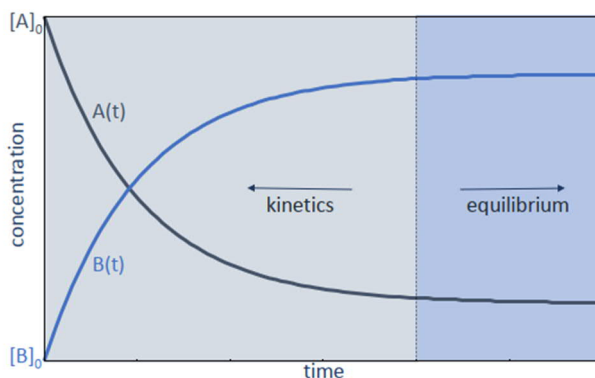


Figure 2.1 Demonstration of the role of “chemical kinetics” and “equilibrium” in the reaction process of $A \rightarrow B$. Reproduced from Tiziano Faravelli, Tsinghua-Princeton summer school on combustion 2022.

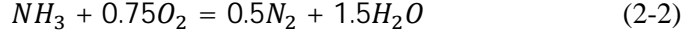
2.1.1 Global reaction and stoichiometry

A global reaction represents the overall chemical equation for the conversion of reactants into products, without detailing the individual reaction steps. The stoichiometric condition is determined by the ratio of fuel to oxidizer required for complete combustion. Equivalence ratio, Φ , is defined as the molar ratio of the fuel to molecular oxygen in relation to the same ratio of a stoichiometric mixture:

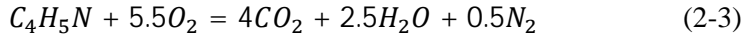
$$\Phi = \frac{n_{(fuel/O_2)}}{n_{(fuel/O_2)_{stoichiometric}}} \quad (2-1)$$

A rich gas mixture has $\Phi > 1$; a lean gas mixture has $\Phi < 1$.

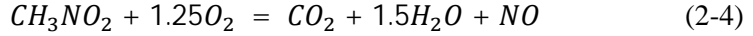
In Papers II–V, ammonia (NH_3) is present in the fuel. Under stoichiometric conditions, nitrogen (N_2) is considered the final product of nitrogen atoms in NH_3 , while water (H_2O) represents the final product of hydrogen atoms. The global reaction for NH_3 combustion with oxygen under stoichiometric conditions is:



In Paper I, pyrrole (C_4H_5N) is the fuel. Under stoichiometric conditions, CO_2 was considered the final product of carbon atoms, N_2 the final product of nitrogen atoms, and H_2O the final product of hydrogen atoms. The corresponding stoichiometric reaction is:



In Paper V, nitromethane (CH_3NO_2) is present in the fuel. Nitrogen oxide (NO) was used as the final product of the nitrogen atom in the stoichiometric equation:



2.1.2 Elementary reactions and rate constant expressions

2.1.2.1 Elementary reactions

In reality, the reactions of the above fuels do not occur in one step as written. Instead, they proceed via a sequence of elementary steps where intermediate species are produced, and each of these individual steps is denoted as an elementary reaction. For example, ammonia requires more than 30 species and 200 elementary reactions to describe its oxidation over a wide range of pressure and temperature [25].

The reactants and products in an elementary reaction may be atoms, molecules, free radicals, ions, excited states, etc. Elementary reactions are fundamental descriptions of how chemical transformations occur. The list of elementary reactions that take place during the course of a global reaction is called the “mechanism” of the reaction [28].

Elementary reactions can be classified based on the number of reactant species that participate in the reaction: A unimolecular reaction involves a single species, describing the dissociation or rearrangement of a single reactant as in the reaction; bimolecular reaction involves two species undergoing a collisional interaction resulting in chemical change; termolecular reaction involves three species interact simultaneously, which is rarer due to lower probability of simultaneous and efficient collisions [28].

Elementary reactions can also be classified by the radical numbers on the reactant and product sides. A radical is an atom or molecule with one or more unpaired valence electrons (outer shell electrons) and is, therefore, much more reactive than nonradical species whose electrons are all paired up. Combustion is dominated by radical chemistry.

Chain-initiating reactions are generally thermal decomposition reactions, which are endothermic because they involve bond breaking, for example, $\text{CH}_3\text{NO}_2 = \text{CH}_3 + \text{NO}_2$. Combustion starts with an initial chain-initiating reaction.

Chain-branching reactions occur when a radical reacts to form two or more radicals, such as $\text{H} + \text{O}_2 = \text{O} + \text{OH}$. This increases the system's reactivity by generating more radicals. Chain-branching reactions are responsible for a flame being self-propagated and are essential in combustion chemistry.

Chain-propagating reactions occur when a reaction generates as many radicals as it consumes, for example, $\text{NH}_3 + \text{OH} = \text{NH}_2 + \text{H}_2\text{O}$. These reactions sustain combustion.

Chain-terminating reactions consume more radicals than they produce, thus reducing the system's reactivity, for example, $\text{NH}_2 + \text{NO} = \text{N}_2 + \text{H}_2\text{O}$.

In an elementary reaction, species interact and transform into other species through bond breaking or formation. The transition state describes the geometry of the interacting species between the reactants and products, representing the highest energy point in the reaction. For a reaction to occur, it must pass through the transition state. The same reactants can give different products when reacting. The branching ratio describes the relationship between different product channels.

2.1.2.2 Empirical rate constant expression

Given an elementary biomolecular reaction:



The forward reaction rate r_f can be written as:

$$r_f = k_f[A][B] \quad (2-6)$$

And the reverse reaction rate r_r can be written as:

$$r_r = k_r[C][D] \quad (2-7)$$

In equations (2-6)(2-7), k_f and k_r are the forward and backward rate constants, respectively. In the expressions the concentration [] are number densities in the units of (*molecules/cm³*), so that the product $[A][B]$ is proportional to the frequency of collisions. The most common empirical expression for the rate constant (k) is:

$$k = A \times T^n \times \exp\left(\frac{-E_a}{RT}\right) \quad (2-8)$$

This equation, known as the modified Arrhenius expression, describes the temperature dependence of the rate constant k . The parameters in equation (2-8) are defined as follows:

- A is the frequency factor, often called pre-exponential factor or “ A factor”, depending on how often molecules collide and whether they are properly oriented. It is a measure of the frequency of effective collisions among the reactants.
- n is the temperature exponent, which accounts for the temperature effect on the A factor.
- E_a is the activation energy, which is the minimal amount of energy required by reactants to undergo a chemical reaction (the difference in energy between the reactants and the transition state).
- R is the universal gas constant, $R=1.987 \text{ cal}/(\text{mol} \cdot \text{K})$.

The reaction rate in equations (2-6)(2-7) is defined as the concentration of the decrease of a reactant per unit time, or the concentration of the increase of a product per unit time. For example:

$$r_f = -\frac{d[A]}{dt} = -\frac{d[B]}{dt} = \frac{d[C]}{dt} = \frac{d[D]}{dt} \quad (2-9)$$

Thus, the unit of rate constants could be deducted based on equations (2-6)(2-7): given the unit of concentration is known and the unit of reaction rate is $\text{mol}/(\text{cm}^3 \times \text{s})$. For a bimolecular reaction, the unit of the rate constants k is $(\text{cm}^3/\text{mol} \cdot \text{s})$; for a unimolecular reaction, the unit for k is $(1/\text{s})$; for a termolecular reaction, k has the unit $(\text{cm}^6/\text{mol}^2 \cdot \text{s})$.

At equilibrium conditions, the net reaction rate is zero, $r_f - r_r = 0$, $k_f[A][B] = k_r[C][D]$. Then, it is possible to determine the equilibrium constant K :

$$K = \frac{k_f}{k_r} = \frac{[C][D]}{[A][B]} \quad (2-10)$$

K is a thermodynamic quantity: by knowing the Gibbs free energy of a reaction ΔG_r from thermodynamic data of each species, the equilibrium constant in pressure units k_p could be calculated through $\Delta G_r = -RT \ln(k_p)$. Therefore, the forward and reverse rate constants k_f and k_r could be deducted from each other with known thermodynamic data.

2.1.2.3 *Rate constant of duplication reactions*

Sometimes, the rate constant shows behavior that cannot be easily explained with one empirical Arrhenius expression in (2-8), and it needs to be expressed as the sum of two Arrhenius expressions.

$$k = A_1 * T^{n_1} * \text{Exp}\left(-\frac{Ea_1}{RT}\right) + A_2 * T^{n_2} * \text{Exp}\left(-\frac{Ea_2}{RT}\right) \quad (2-11)$$

These reactions are denoted as duplication reactions, which have two sets of Arrhenius parameters.

2.1.2.4 *Rate constant of pressure-dependent reactions*

Some reaction rate expressions depend on pressure as well as temperature, particularly unimolecular decomposition, recombination, and complex-forming bimolecular reactions [29]. For a unimolecular dissociation reaction in the form:



It could be split into two steps according to the Lindemann mechanism [29]:



The first step involves a “strong” collision between a bath gas molecule (M) and a reactant molecule AB, transferring enough energy to excite AB into a higher-energy state above the reaction barrier (excitation). This energized species, AB*, can then either proceed to form products A + B (reaction) or lose energy through another collision, returning to AB (deactivation). After a short period, the rates of formation and loss of AB* balance out, and its concentration ([AB*]) reaches a steady-state value, meaning $d[AB^*]/dt=0$. Not all the molecules are equally effective as collisional partners; some are more effective than others. Thus, the enhanced collisional efficiency of the molecules should be denoted.

Assuming that the time required to achieve the steady-state condition is negligible compared to the total reaction time, then the apparent unimolecular rate constant for the reaction $AB \rightarrow A+B$ can be derived, as described in Figure 2.2. At high pressure, when there are a lot of molecules around and $[M]$ is high, the rate constant converges to a constant called “high-pressure limit k_∞ ”. At sufficiently low pressures, the rate constant is proportional to $[M]$, and the rate constant at this region is called “low-pressure limit k_0 ”. The correlations between the high-pressure and low-pressure limits and $[M]$ are available in many works, such as [29-31], and thus are not discussed in detail.

The rate constant of a unimolecular three-body reaction variation with pressure is described in Figure 2.2. The “fall-off region” refers to the transitional phase where the reaction rate shifts from a linear dependence on pressure to becoming

independent of pressure. Many reaction systems fall in this region. The fall-off region could be expressed in *Troe* format [32] and *PLOG* format [33]. In the *PLOG* format, the actual rate constant k at a pressure p is obtained by performing linear interpolation in $\ln(p)$ between the tabulated pressure points:

$$\ln k = \ln k_i + (\ln k_{i+1} - \ln k_i) \frac{\ln p - \ln p_i}{\ln p_{i+1} - \ln p_i} \quad (2-15)$$

The *Troe* format describes the fall-off region using high- and low-pressure limits k_∞ and k_0 , as well as a temperature-dependent function. This function includes four constants to characterize the temperature dependence of the fall-off region curve.

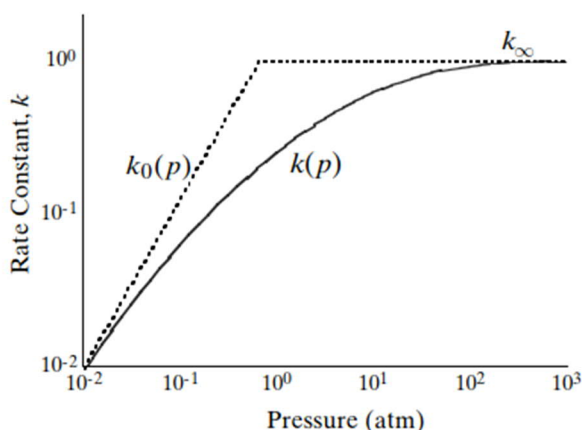


Figure 2.2 Characteristic variation of a unimolecular reaction rate constant with pressure. Reproduced from [31].

2.2 Chemical kinetic model and determination of rate constants

2.2.1 What is a chemical kinetic model?

A chemical kinetic model contains species with associated thermodynamic and transport properties, elementary reactions, and associated rate constants.

Thermodynamic properties of each species include standard enthalpy of formation (Δh_f^0), standard entropy of formation (S_0), and heat capacity (C_p), with their

dependence on temperature, in polynomial form. The reactions are commonly presented with rate constants in one direction. The software calculates the reverse rate from the thermodynamic properties of the species involved and the forward rate constant.

The transport properties of species are required for problems involving diffusion, convection, or conduction, such as in flames. These properties characterize the molecular transport of species, momentum, and energy. Transport properties of a species include diffusion coefficients, viscosities, thermal conductivities, and thermal diffusion coefficients. In laminar flames, diffusion plays an important role due to concentration gradients.

Developing a detailed kinetic model is often hierarchical and modularized [1, 34]. A large model is hierarchically assembled based on several sub-mechanisms built upon each other, starting with those involving smaller species. This strategy allows the modeler to avoid building the entire model from scratch; instead, they can focus on specific sub-mechanisms for targeted species and integrate them into an already validated core, the base mechanism, similar to solving a puzzle piece by piece.

Therefore, each of my works investigates different modules within nitrogen-containing species chemistry rather than examining the whole. To achieve this, each study explored different mixtures, expecting that composition variations would change the radical pools within the flames, leading to different dominant chemistry.



Figure 2.3 A picture of Prof. Alexander Konnov's office. Chemical kinetic modeling works are classified by different modules.

My research focuses on validating and updating or developing the chemical kinetic model developed by Prof. Alexander Konnov and his colleagues. This kinetic model has been continuously and iteratively updated for about 25 years of research activity. In this study, the starting model for developing ammonia chemistry was taken from the work of Han et al. [35], published in 2021, and contains the latest H/N/O chemistry developed by our group. The starting model for developing pyrrole chemistry is from the work of Alekssev et al. [36], published in 2022, which contains the latest C/N/H/O chemistry. The transport and thermodynamic properties of the species in ammonia chemistry were not examined during the course of the work presented in the thesis, but were accepted as is in the mechanisms. The thermodynamic data for most ammonia and hydrocarbon chemistry species are sourced from the Burcat and Ruscic database [37]. The transport properties for most species in ammonia chemistry are taken from the Chemkin transport database, which are also used in many existing ammonia chemical kinetic models. For hydrocarbon species, the transport data are primarily based on the work of Jasper et al. [38, 39]. For Papers I and V, in the absence of thermodynamic and transport data of related species in the model of pyrrole and nitromethane, these data were evaluated or selected from the literature.

2.2.2 Determination of rate constants

The reaction rate constant can be determined through theoretical calculations and direct experimental measurements of intermediate species and their concentrations. In the absence of numerical or measured values, analogy methods and estimations can be made.

Both theoretical calculations and direct measurements have their difficulties. To briefly explain why, I will cite Egolfopoulos et al.'s review [40]. For the theoretical calculation, *“the presence of unknowns frequently exceeds the number of equations, given the limited knowledge on the quantum states, potential energy surface, anharmonicity and the third body collisional energy transfer”*. Direct experimental measurements in a broad parametric range with confidence is also challenging, due to *“equipment limitation in capturing accurately events of intermediate species at the (sub)-picosecond level and in the unavoidable coupling with other reactions”*.

Therefore, the accuracy of the chemical kinetic model requires validations using fundamental experiments. Meanwhile, as there is no universal knowledge of the correct chemistry behind each fuel, the choices in species and reaction included in a model constitute one of the differences between kinetic models; thereby, fundamental experiments also help select rate constants among literature.

2.3 Chemical kinetic model validations

The fundamental experiments in the combustion research field could scrutinize the chemical kinetics problems and simplify and minimize complicated physical problems in mixing, flow, and heat transfer. Thus, they are also often called fundamental chemistry experiments. Fundamental experiments at present mainly include “kinetic reactors” and laminar flames. Each type of experiment has limited operating temperature and pressure ranges, and by combining them, one can validate the chemical kinetic models over wide temperature and pressure ranges pertinent to practical combustion applications.

Kinetic reactor systems include shock tube (ST) and rapid compression machine (RCM), plug flow reactor (PFR), jet-stirred reactor (JSR), and so on. These systems have the advantage of being free from transport effects, simplifying the modeling procedure.

Laminar flames for model validations are typically low-dimensional and stable. Under these conditions, the processes of heat and mass transport give rise to more complex interactions among various species, potentially highlighting different reaction pathways. Laminar, premixed, one-dimensional (1D) flames are my research focus.

Table 2.1. Fundamental combustion experiments, apparatuses, and measuring targets used for model validations in this study.

Fundamental combustion experiments	Apparatuses	Measuring targets
Premixed, 1D, laminar flames (my research focus)	Heat flux burner, spherical combustion bomb	Laminar burning velocity
	Porous-plug McKenna burner, heat flux burner	Flame structure
Kinetic reactors	Shock tube (ST)	Ignition delay times, Speciation profiles
	Jet-stirred reactor (JSR)	Speciation profiles
	Plug flow reactor (PFR)	Speciation profiles

Table 2.1 lists the fundamental experiments and their measuring targets used in my study for model validations. The laminar burning velocities and the ignition delay times are global combustion characteristics, representing the overall reactivity of a mixture. In contrast, the speciation profiles and flame structure are micro-scale combustion characteristics and serve as more stringent validation targets. As mentioned before, developing a detailed kinetic model follows a modular approach. Since my primary experimental focus is on laminar burning velocities governed by high-temperature chemistry, literature experiments conducted under similar temperature conditions were frequently used for validation, such as shock tube

studies. Other systems, such as rapid compression machines, plug flow reactors (PFRs), and jet-stirred reactors (JSRs), were used less often for validation, as they typically operate at relatively lower temperatures.

2.3.1 Laminar flame experiments

2.3.1.1 *Laminar flame structure*

The structure of a premixed laminar flame can be separated into four zones according to Figure 2.4: the unburned gas zone, the preheat zone, the reaction zone, and the product zone.

In the unburned zone, the fuel and oxidizer are uniformly mixed but do not react. The temperature is not sufficiently high to initiate the combustion process.

In the preheat zone, the gas mixture is still unburned, but the temperature rises through heat from the reaction zone. The rising temperature can initiate the initial reactions, such as the decomposition of the fuel. The boundary between the preheat zone and the reaction zone is often defined as the position at which an inflection point exists in the temperature profile.

Exothermic reactions mainly occur in the reaction zone. The fast release of energy in a very narrow region leads to a very steep temperature gradient. Because of the high temperature, fuel degrades to short fuel fragments or radicals. This leads to a rich mix of reactive species. Intermediate species are produced and consumed at a high rate, driven by the high temperature. The temperature reaches its peak just behind the reaction zone before stabilizing into a plateau. A reaction zone is often called a flame front. The visible region generally occurs near the peak of the temperature profile, where enough energy is released to excite species.

The recombination reactions occur at the beginning of the post-flame zone and start directly after the reaction zone. Further away in the post-flame zone, equilibrium gas concentration will be reached. The species composition in the product gas will depend on the equivalence ratio. A stoichiometric mixture typically consists of nitrogen, carbon dioxide, and water.

The flame structure of $\text{NH}_3+\text{O}_2+\text{Ar}$ mixtures was measured in Paper IV, using a porous-plug McKenna burner for flame stabilization, coupled with the optic diagnostic technique, Raman Spectroscopy. My colleague, A. Zubairova, carried out the experiments while I focused on the chemical kinetic modeling parts. Therefore, a detailed methodology will not be presented here but will be included in A. Zubairova's doctoral thesis.

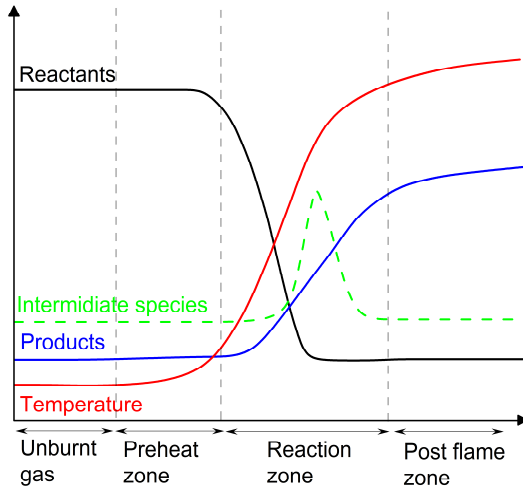


Figure 2.4 Schematic of the flame structure of a flat 1D premixed laminar flame.

2.3.1.2 Laminar burning velocity

Laminar burning velocity (LBV) in the study is a well-defined quantity: it is “the flame propagating speed of a premixed, laminar, one-dimensional, adiabatic flame with zero stretch” [41]. The term “adiabatic” describes an ideal process that occurs without energy exchange. In real flames, the adiabatic velocity is the velocity where the net heat interactions with the surroundings are zero. An adiabatic flame temperature is the temperature a flame would reach without any heat loss to its surroundings. Flame “stretch” is caused by a change in the area of the propagating flame front with time due to aerodynamic and boundary conditions [41]. When the flow of the unburned gas is equal to the flame's consumption rate, a stationary flame is created that is unaffected by stretching.

LBV of a given fuel depends on the stoichiometric ratio, pressure and temperature only. LBV is the “elemental unit” in describing complex combustion phenomena, such as turbulent flame speed, flame flashback, etc. [42]. Accurate values of LBV are equally crucial for practical applications, e.g., they often serve as an input parameter for the CFD models [43].

Different methods, such as heat flux burner, spherical combustion bomb, and counter flow burner, could measure the LBV. In my thesis, the heat flux burner setups at Lund University were used for LBV measurements, which are applicable for atmospheric pressure measurements, and details are in Chapter 3.

2.3.1.3 Temperature and pressure dependence

Practical applications of combustion often take place in environments that have elevated temperatures and pressures compared to the standard conditions. These environments present challenges for fundamental experiments, as they require large-scale apparatus, introduce more complex safety concerns, and make it more difficult to maintain well-defined flames [44]. For this reason, studying the temperature and pressure dependence effect on the LBV is helpful to allow extrapolation of the measured LBV from lab-achievable conditions to desired conditions.

In addition, temperature and pressure dependence factors can serve as additional validation targets; a detailed analysis by Konnov [45] on these factors for methane and hydrogen flames found that the power exponents α are not very sensitive to the rate constants implemented in the modeling; therefore they are more suitable for analysis of consistency of the measurements among different labs and helps to check that the data are not biased by some systematic or random errors.

In this study, temperature and pressure dependence factors are not the primary focus. Only in Paper III was the temperature dependence examined, specifically to assess data consistency across different studies for the LBV of $\text{NH}_3+(\text{O}_2+\text{N}_2)$ mixtures. The correlation describing the effect of temperatures is given by [41]:

$$LBV = LBV_0 \times \left(\frac{T_g}{T_g^0}\right)^\alpha \quad (2-16)$$

where LBV is the burning velocity at a specific unburned gas temperature T_g . LBV_0 is the burning velocity at a reference temperature T_g^0 . The power exponent α is a single scalar quantity. With increasing temperature, $\alpha > 0$ indicates that LBV increases with temperature.

In this study, calculations of α and its uncertainty used a MATLAB code developed by Alekssev et al. [46]. α was calculated using least squares model, and is a function of individual LBV at each temperature T_g^i , i.e., $\alpha = f(LBV_{T_g^1}, \dots, LBV_{T_g^n})$, where n is the number of data points. α at each temperature was estimated using:

$$\alpha_{T_g^i \rightarrow T_g^0} = \frac{\ln(LBV/LBV_0)}{\ln(T_g^i/T_g^0)} \quad (2-17)$$

The uncertainties $\Delta\alpha$ were estimated with the error propagation rule, with a simple linear regression model:

$$\Delta\alpha = \frac{\left(\sum_i \left[\left(\ln \frac{T_g^i}{T_g^0} - \overline{\ln \frac{T_g^i}{T_g^0}} \right) \times \frac{\Delta LBV^{T_g^i}}{LBV^{T_g^i}} \right]^2 \right)^{0.5}}{\left(\sum_i \ln^2 \frac{T_g^i}{T_g^0} - n \times \left(\overline{\ln \frac{T_g^i}{T_g^0}} \right)^2 \right)} \quad (2-18)$$

Where $\Delta LBV^{T_g^i}$ is the uncertainty of the burning velocity at temperature T_g^i . $\overline{\ln \frac{T_g^i}{T_g^0}}$ is mean logarithmic normalized temperature:

$$\overline{\ln \frac{T_g^i}{T_g^0}} = \frac{\sum_i \ln \frac{T_g^i}{T_g^0}}{n} \quad (2-19)$$

2.3.2 Other fundamental experiments

Literature fundamental combustion data from shock tubes, jet-stirred reactors, and plug-flow reactors are also used as validation targets for more comprehensive model validation. Thus, the characteristics of these experiments are also briefly introduced here.

2.3.2.1 Shock tubes

Shock Tube is designed for high temperature autoignition studies, using shock waves to generate the target temperature and pressure conditions for ignition delay time (IDT) measurements. Fuel autoignition refers to the spontaneous ignition of fuel under specific temperature and pressure conditions that enable combustion. The process begins with a short preparatory phase, that is ignition delay time (IDT). During this early stage, fuel molecules undergo chemical bond breakage, leading to the formation of reactive free radicals. Eventually, ignitions occur, marked by a rapid rise in pressure and temperature. The ignition delay time is a fundamental combustion property and a key parameter in designing combustion systems and developing kinetic models. A shock tube combined with optical diagnostics can provide speciation validation targets. In Paper II, speciation data during NH_3 pyrolysis and oxidation in shock tubes played an important role in helping select rate constants from literature.

2.3.2.2 Jet-stirred reactors and plug-flow reactors

The jet-stirred reactor (JSR) is a type of ideal continuously stirred-tank reactor well suited for gas-phase kinetic studies. Jet-stirred reactor studies consist of recording the evolution of the reactants' conversion and the mole fractions of reaction products

as a function of different parameters such as reaction temperature, residence time, pressure, and composition of the inlet gas [47]. The plug-flow reactor (PFR) system is a model used to describe chemical reactions in continuous, flowing systems of cylindrical geometry [48].

In the PFR, chemical reactions are carried along with the flow, and there is no back-mixing of product species. In contrast, a JSR represents an idealization where combustion products are back-mixed with reactants so quickly that the reaction zone is distributed uniformly in space [48]. Therefore, in a JSR, no gradients in temperature or species exist, and the combustion region can be characterized by a single value for temperature and all species. Because all the reaction products are back-mixed with the reactants, the chemical pathways for combustion and pollutant formation can be different than in purely premixed or diffusion flames [48].

Jet-stirred reactors and plug-flow reactor systems have found widespread application in combustion chemistry studies because the combustion characteristics can be measured as a function of a single coordinate (time or space). Correspondingly, the respective computer simulations can employ zero- or one-dimensional combustion models with detailed mechanisms [48].

3 Experimental method - the heat flux method

This chapter introduces the experimental methodology of the heat flux method used in my thesis. The experimental apparatus, LBV determination method, and uncertainty analysis were developed by former colleagues in our research group and are detailed in the work of Vladimir A. Alekseev et al. [49], which serves as the primary reference for this section.

The heat flux method was first introduced in 1993 by de Goey et al. [50], and later thoroughly analyzed by Bosschaart and de Goey [51]. They implemented a major modification to the flat flame burner setup, enabling the determination of flame heat loss to the burner—essential for flame stabilization—as a function of the inlet velocity. By interpolating or extrapolating the results to the point of zero net heat transfer, they were able to approximate adiabatic flame conditions. de Goey et al. [50] validated that the flame structure near the reaction layer is equal to that of a modeled adiabatic flame with initial temperature equal to the gas temperature in the mixing chamber. Since their work, the heat flux method has been widely adopted by various research groups. The core components of the heat flux burner setup and the data processing procedures have remained largely consistent across laboratories [49], including in our own research group.

One of the key advantages of the heat flux method is that it produces a flame that is approximately adiabatic and free from flame stretch effects, eliminating the need for further flame stretch correction. However, the heat flux method has certain limitations in its measurement range, as noted in the review by Konnov et al. [41]: 1) when applied to mixtures with laminar burning velocities exceeding 80 cm/s. In such cases, the burner hole size must be reduced to make sure the gas flows from each hole merge before reaching the flame front, thereby allowing a flat flame to form. However, this requirement makes fabrication more challenging; 2) measurement of laminar burning velocities at higher mixture temperature is difficult as the flame velocity increases and flame stand-off distance (the distance from the reaction zone to the burner plate surface) reduces, resulting in increased radical quenching over the plate; 3) at high pressures, burning velocities are very low and flame stabilization becomes difficult beyond 10 atm. The heat flux method was developed for LBV measurements of gas and liquid fuels, with air or modified oxidizers, at room or elevated initial temperatures. It could be applied to

atmospheric pressure and elevated pressures in some labs [52]. The heat flux burner setups at Lund University were limited to atmospheric pressure LBV measurements.

Other common LBV measurement methods include the spherical flame method, counterflow flame method, and the conical (Bunsen) flame method, and so on. These methods can extend the investigation temperature or pressure ranges. Literature LBV data from the spherical flame method are commonly used as validation targets in my study. The conical flame method has notable disadvantages, such as its nonadiabatic nature and air entrainment into the flame cone base, thus can only be used for a rough estimation of the LBV [53]. In the spherical flame method, the fuel + air mixture is ignited at the center using a spark, and flame propagation speed is determined either from pressure-time history or flame radius with time. In the counterflow flame method, the minimum flow velocity near the stabilized flame is considered as flame propagation velocity. Both the spherical flame method and the counterflow flame method suffer from flame stretch, requiring flame stretch corrections to determine laminar burning velocity.

As summarized by Konnov et al. [41], the LBV of methane and air mixtures, as measured by the heat flux method, spherical flame method, and counterflow flame method, has converged in recent years to approximately 36 ± 1 cm/s at the stoichiometric condition. Although these methods are based on different principles and influenced by varying sources of uncertainty, this convergence validates that the assumptions underlying each technique are sufficiently accurate to support a unified definition of LBV.

3.1 The apparatus

A schematic of a typical heat flux burner setup is shown in Figure 3.1. The setup can be divided into four main parts: (A) liquid and gas preparation, (B) flow control and mixing, (C) temperature control, and (D) LBV measurements.

At Lund University, two independent heat flux burner setups are available, referred to as “Panel 1” and “Panel 2”. Figure 3.1 shows the scheme of “Panel 1”, while both setups share the same fundamental structure, but “Panel 2” is equipped with only two gas lines and has a smaller evaporator capacity. Typically, “Panel 2” is used for corrosive liquid fuel measurements (Paper I).

In parts A and B of Figure 3.1, all gas lines are supplied from either a central gas system or gas bottles located in the laboratory. Each line is equipped with specific filters upstream of the mass flow controllers (MFCs) to ensure clean operation. For safety issues, plug valves are installed both upstream and downstream of the MFCs to enable isolation in the event of uncontrolled flow. A 3 L buffering tank is used before the gas lines to stabilize the flow and mitigate sudden pressure fluctuations

Parts C and D are the essential parts for obtaining LBV. After flow and mixing, the prepared gas mixture is delivered to the heat flux burner via a 2-meter-long heating hose (KLETTI GmbH). The heating hose is maintained at a specific temperature for experiments involving liquid fuels or diluents to prevent condensation.

A typical heat flux burner could be divided into three parts: plenum chamber, burner head, and burner plate. All three components are made of brass. Their goal is to create a uniform flow (in terms of velocity and temperature) towards the burner plate. A cross-sectional view of a typical heat flux burner is shown in Figure 3.2 (a), and the burner plate is shown in Figure 3.2 (b). All the heat flux burners in this study are designed and manufactured at the Eindhoven University of Technology.

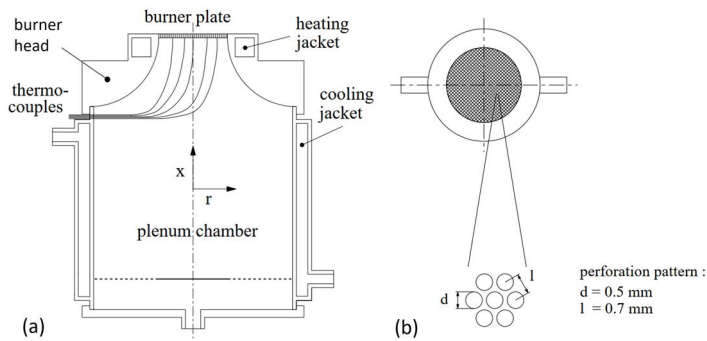


Figure 3.2 Illustration of a heat flux burner: (a) the cross-sectional diagram and (b) the burner plate, reproduced from [54].

In the plenum chamber, a perforated plate is placed inside at a distance from the bottom, which is used as a flow straightener. The plenum chamber's outer cooling jacket is connected to a thermostatic water bath (Grant Instruments, model GD120) to keep the unburned gas at a constant temperature, T_g .

The burner head holds the burner plate on the top, whose heating jacket is connected to another thermostatic water bath (of the same type). This temperature of the heating jacket (T_{hj}) was set at least 30 K above the unburned gas T_g . The difference between T_{hj} and T_g is an important factor for flame stability, which will be discussed below in section 3.4. The hotter part of the burner head is thermally insulated from the bottom part of the burner head with a ceramic ring so that the unburned gases are expected to be kept as T_g before entering the burner plate.

The burner plate, shown in Figure 3.2 (b), is a 2-mm-thick brass plate with multi-hole perforation. Depending on the burner model, the burner plate can be attached

directly to the burner head during manufacturing or adhered to the burner head by thermal paste. The hole diameter d and pitch l also vary by design; typically, d is 0.5 mm, and l is 0.7 mm. The burner plate is inserted with at least eight thermocouples, each thermocouple inserted in each of the holes to monitor the radial temperature distribution. In our burners, E-type and T-type thermocouples are commonly used, with measurement errors of approximately $\pm 1^\circ\text{C}$ and $\pm 1.7^\circ\text{C}$, respectively.

Determination of the LBV in flat flames stabilized at adiabatic conditions is carried out by obtaining one radial temperature fitting parameter as a function of the inlet unburned gas velocity (details are below), using a LabVIEW script.

3.2 Principle and LBV data processing method

3.2.1 Principle

In the heat flux method, adiabatic conditions are achieved when the heat loss from the flame to the burner, necessary for its stabilization, is compensated by the heat gain to the unburned mixture as it enters the preheated burner plate. As the name suggests, the method requires a balance in the heat flux. The heat flux principle is shown in Figure 3.3; the left arrows indicate the gas flow direction, and the right arrows show the heat transfer between the flame front, the burner plate, and the unburned gas flow.

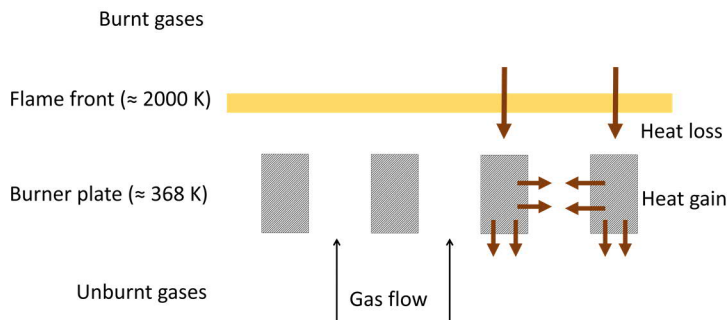


Figure 3.3 Heat flux principle

The most relevant variable in this method is the burner plate temperature profile, which detects heat loss and heat gain of the flame. The radial temperature distribution in the burner plate is in the form of:

$$T_r = T_{center} - \frac{q}{4\lambda h} r^2 = T_{center} + C \times r^2 \quad (3-1)$$

where T_{center} is the temperature of the central point, q is the net external heat transfer per unit area to (or from) the burner plate, λ is the thermal conductivity of the plate in the radial direction, and h is the thickness of the plate. The net heat transfer, q , is the difference between the heat transferred to the burner plate from the flame (q_+) and the heat transferred from the plate to the preheating gas (q_-), i.e.:

$$q = q_+ - q_- \quad (3-2)$$

The quantity $-q/4\lambda h$ is called the parabolic coefficient, C , which is the method's key parameter. During the measurements, C was obtained from the measured temperature distribution in the burner plate by fitting to equation (3-1). When adjusting the unburned gas velocity V_g , the net heat transfer q will get affected:

$$q = \rho_u V_g C_p (T_{ad} - T'_b) \quad (3-3)$$

Where T_{ad} is the adiabatic flame temperature and T'_b is the actual flame temperature at V_g ; ρ_u is the unburnt gas density and C_p is the specific heat. As a result, the parabolic coefficient C will also be affected:

When $V_g = LBV$, $T'_b = T_{ad}$, $q = 0$, i.e., there is no net heat transfer between the burner plate and the flame. At this point, $C = 0$, and a uniform radial temperature profile could be observed in the burner plate.

When $V_g < LBV$, $q > 0$, i.e., $q_+ > q_-$, the heat loss from the flame to the burner plate is bigger than the heat gained from the plate to the unburnt gas. At this point, $C < 0$, this state is called a sub-adiabatic condition, where the radial temperature increases toward the center of the burner plate.

The opposite conditions when $V_g > LBV$, $q < 0$, $C > 0$ are called super-adiabatic; where the radial temperature decreases toward the center of the burner plate.

Figure 3.4 shows the temperature distribution on the burner plate and corresponding parabolic coefficient C for a sub-adiabatic and super-adiabatic condition, during the experiments for $\text{NH}_3 + \text{O}_2 + 40\% \text{ Ar}$ flame in Paper II.

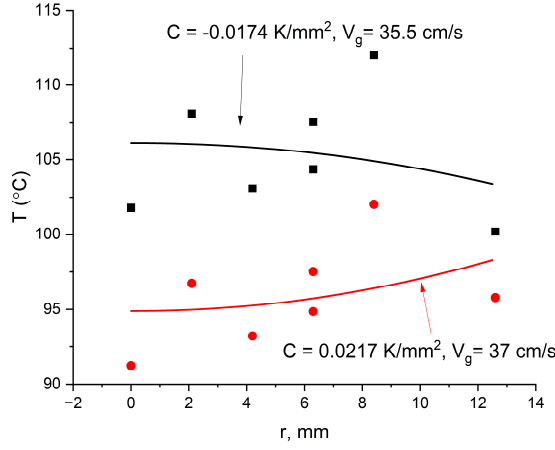


Figure 3.4 Temperature distribution in the burner plate for $\text{NH}_3 + \text{O}_2 + 40\% \text{ Ar}$ flame in Paper II. Symbols: experimental, lines: parabolic fit to equation (3-1).

3.2.2 LBV data processing method

By obtaining parabolic coefficient dependence C as a function of inlet gas velocity V_g , the laminar burning velocity, LBV, could be found by linear interpolation of the points in the vicinity of the state $C = 0$:

$$\text{LBV} = V_g|_{C=0} \quad (3-4)$$

Figure 3.5 shows this process using interpolation. A MATLAB code developed in our research group [49] was used for the data processing of LBV. In [49], Alekseev et al. concluded that 4-5 points of V_g in a 2 cm/s interval are sufficient to damp any random scatter of the parabolic coefficient while still being within the local linearity of $C(V_g)$.

V_g could be obtained by dividing the total flow rate of MFCs, ϕ_{tot} , by the cross-section of the flow, A . According to the ideal gas law:

$$V_g = \frac{p_0}{p} \cdot \frac{T_g}{T_0} \cdot \frac{F_{tot}}{A} \quad (3-5)$$

Where F_{tot} is expressed in normal liters per minute (L_n/min) under standard pressure p_0 and temperature T_0 (0°C , 1 atm), while p is the actual pressure during the measurements, and T_g is the temperature of unburned gas. The total flow rate

F_{tot} is calculated by the LabVIEW script using its relation to V_g (the input parameter in LabVIEW).

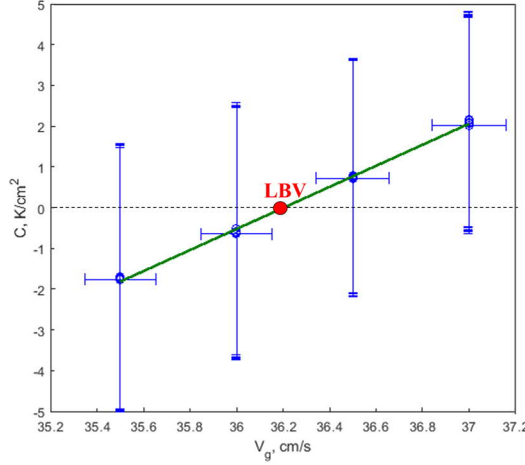


Figure 3.5. Determination of the LBV from $C(V_g)$ dependence using interpolation for the $\text{NH}_3 + \text{O}_2 + 40\% \text{ Ar}$ mixture at $\Phi=0.9$, 298 K in Paper II.

Notice that ideally this location of $C = 0$, $\text{LBV} = V_g$ is found by linear interpolation. However, in some cases, extrapolation from sub-adiabatic conditions is necessary. This happens when the flame front shows some instabilities around adiabatic conditions and easily suffers from “cell formation”, as will be introduced in section 3.4. In case when cellular structures are formed near the adiabatic conditions, the propagation speed of adiabatic cellular flame is higher than the laminar burning velocity due to increase of the flame surface area, making it impossible to find LBV by interpolation. Therefore, the points where the flames are not flat had to be filtered out, which normally could be observed during experiments. Based on the remaining points, LBV had to be obtained by fitting the extrapolation line.

An illustration case of the extrapolation process is shown in Figure 3.6. In the case of extrapolation, C might not be perfectly linear to V_g . A modified method of data processing needs to be used [49]. Instead of directly plotting C as a function of V_g , a normalized relative quantity $C_r = C/V_g$ was used, and C_r is proportional to V_g [49].

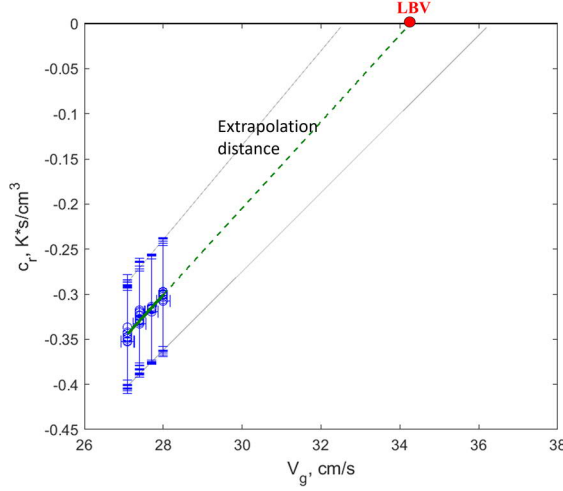


Figure 3.6 Determination of the LBV from $C_r(V_g)$ dependence using extrapolation, for the $\text{CH}_3\text{NO}_2 + \text{air}$ mixture at $\Phi=1.0$, 338 K in Paper V.

The extent of extrapolation (extrapolation distance) between experimental points varies depending on temperature and equivalence ratio. In general, flames were more prone to developing cellular structures as the unburned gas temperature increased and for rich mixtures with equivalence ratios greater than 1.

However, the extrapolation distance is limited. When extrapolating from a distance that is too far from adiabatic condition, it means that the flame velocity is much larger than inlet velocity V_g , making the flame closely attached to the burner plate. This results in excessive heating, which can potentially damage the attachment of the burner plate to the burner head, particularly when the plate is adhered by thermal paste, which has a melting point around 250°C.

When the LBV of a mixture is higher, it needs to be extrapolated from a farther distance to avoid flame corrugation. However, the above-mentioned limitation on the maximum allowable extrapolation distance restricts the LBV measurements in this case. This issue was relevant in the measurements of CH_3NO_2 and NH_3 mixtures at 338 K in Paper V, where the maximum measurable LBV was constrained by the extrapolation distance.

3.3 Uncertainty sources

In [49], all the possible uncertainty sources arising from each part of the setup were identified and discussed, including 22 issues. After detailed analysis, they approximately quantified the expected variations in burning velocity (ΔLBV) due to each of the uncertainties.

Among these factors, the thermocouple scattering and the mass flow control, are generally seen in the literature as the main factors contributing to the total uncertainty of the laminar burning velocity [49]:

1) Thermocouple scattering directly affects the error in fitted parameter C . At a condition near $C = 0$, where the temperature distribution should be uniform, thermocouple scattering is bigger if the maximum temperature difference over the burner plate is bigger. According to equation (3-1), the standard error of the fitted parameter C , σ_C , brought by thermocouple scattering is:

$$\sigma_C = \sqrt{\frac{\frac{1}{n-2} \sum_{i=1}^n (T_i - C \cdot (r^2)_i - T_{\text{center}})^2}{\sum_{i=1}^n [(r^2)_i - (\bar{r}^2)]^2}} \quad (3-6)$$

where n is the number of thermocouples, T_i are thermocouple readings at radial r_i , and \bar{r}^2 is the average of the squared radius. ΔLBV due to thermocouple scattering (ΔLBV_{TC}) is:

$$\Delta LBV_{TC} = \frac{\sigma_C}{s} \quad (3-7)$$

Where s is the parabolic coefficient sensitivity, $s = \frac{dC}{dV_g} \big|_{V_g=LBV}$, which is the slope of the curve in Figure 3.5 and Figure 3.6 at $V_g = LBV$.

2) Mass flow control uncertainty was controlled by calibrations on gas MFCs before the measurements. A drum-type gas meter (Ritter TG10/5) was used for MFCs calibration in this study. Calibration curves, expressed as fourth-degree polynomials were introduced into the LABVIEW operating program to correct the flow rates before being sent to MFCs. The drum-type gas meter provides $\pm 0.5\%$ accuracy in the gas flow rate. Thus, ΔF_i , the uncertainty in the flow rate of each gas component “i”, is the sum of 0.5% stated accuracy plus the stated 0.2% flow repeatability of the MFC, resulting in 0.7% in total. For the liquid Coriolis flow meters, the stated accuracy is around 0.2%. The uncertainty in LBV due to flow rate measurement (ΔLBV_{MFC}) is equal to:

$$\Delta LBV_{MFC} = LBV \times \frac{\sqrt{\sum (\Delta F_i)^2}}{F_{tot}} \quad (3-8)$$

F_{tot} is the total flow rate of MFCs. For the uncertainty in equivalence ratio ($\Delta\Phi$), the error propagation rule gives the following expression for a single fuel:

$$\Delta\Phi = \Phi \sqrt{\left(\frac{\Delta F_F}{F_F}\right)^2 + \left(\frac{\Delta F_O}{F_O}\right)^2} \quad (3-9)$$

Where subscript F and O correspond to fuel and oxidizer.

During the experiments, the thermocouples' readings, the fitted parabolic coefficients C , the number of MFC used, and the calibration method were all recorded in LABVIEW. In the data processing procedure, using a customized MATLAB code developed in [49], the LBV at each condition, the associated uncertainties in the above factors, and their contribution to the LBV uncertainty and equivalence ratio uncertainty will be calculated.

Since the laminar burning velocity is obtained by linear regression of the recorded $C(V_g)$ dependence, the code also includes the uncertainty in the determination of C at $LBV=V_g$ by the regression equation. The extrapolation process normally brings higher uncertainty compared to interpolation. The extrapolation process in Paper V was found to contribute with ~ 0.2 cm/s to the overall uncertainty in the laminar burning velocity.

3.4 Flame instabilities and fuel corrosivity

3.4.1 Flame instabilities

In this study, the LBV investigation range was limited to 15–60 cm/s. At higher velocity, the flame homogeneity might be disturbed by a nonuniform velocity profile; since the heat flux method utilizes a perforated burner plate, local flow distortions are introduced. At high V_g , these distortions can perturb the flame front, increasing the flame surface area due to corrugation. For the common perforation patterns used in our lab's burner plate, the upper limit of V_g is approximately 60 cm/s. This constraint applies to Papers *II* and *III*. When V_g is too low, the flames might be too weak to be stabilized as a flat flame.

Additionally, flame stability is hindered by cellular structures, where the flame front forms “cells” that prevent accurate LBV measurements. Cellular structures typically arise when the unburned gas mixture temperature increases or when the mixture is fuel rich. Literature identify two primary causes of cellularity: hydrodynamic and diffusive-thermal instabilities [55, 56]. Hydrodynamic instabilities occur due to flame front amplification caused by density variations resulting from thermal expansion of the burned gas. Diffusive-thermal instabilities arise when the mass

diffusivity of the deficient reactant exceeds its thermal diffusivity. This commonly occurs in fuel-rich flames of long-chain hydrocarbons or fuel-lean hydrogen flames.

Increasing the temperature difference between the burner plate and the unburned gas mixture can help suppress cellular formation. Experimental studies suggest that this temperature difference should be at least 30 K. In our setup, the burner head temperature was fixed at 368 K (95°C), approximately the highest possible temperature allowing water circulation without evaporation. Consequently, the plenum chamber temperature—corresponding to the unburned gas temperature for investigation—should ideally not exceed 338 K (65°C). Except for Paper *III*, where the maximum investigation temperature was set to 348 K, all experiments adhered to this limit. Although this temperature approached the threshold, no cellular structures were observed, making the measurements feasible.

Figure 3.7 (a) provides visual examples of different flame conditions: (a) a weak flame, with the red circles highlighting its edge as it begins to lift off; (b) a stable flat flame, representing the ideal condition for LBV measurements; (c) A case of flame corrugation, with the affected area highlighted in red circles.

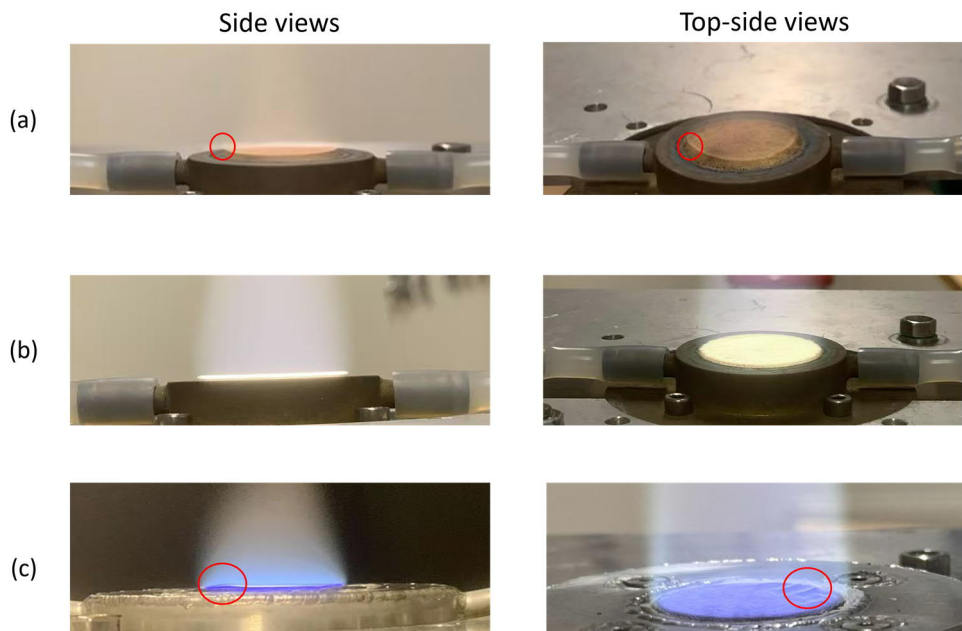


Figure 3.7 Side views and top-side views of three flames (a) a weak flame; (b) a flat flame for LBV measurements (c) a corrugated flame.

3.4.2 Fuel corrosivity

This study involves the use of pyrrole and ammonia, both of which are corrosive chemicals that react with brass, the material used in all burners. As a result, two specific burners, referred to as burner “E2” and burner “T”, were selected for the experiments. These burners have been frequently used in previous studies for measurements involving corrosive fuels.

After each operation with corrosive fuels, the two burners, along with the flow mixing system, were cleaned by flowing CH_4 +air mixtures, and the burners’ performance was assured by measuring the LBV of CH_4 /air or ethanol/air mixtures, as mentioned in each paper.

It is well known that ammonia tends to adsorb onto metal surfaces. This leads to two primary concerns: 1) Deviation of the actual NH_3 feed rate: NH_3 can be adsorbed on stainless steel surfaces upstream of the burner, potentially causing a discrepancy between the flow rate set by the MFC and the actual amount entering the flame; 2) Interaction with burner materials: Adsorbed NH_3 may react with the brass components of the burner chamber, potentially altering the mixture composition and flame structure downstream.

Regarding the first concern, it was concluded that the NH_3 concentration was not affected, as the measurements showed high repeatability across different time intervals. No irregular flame instabilities or fluctuations in the measurements were observed during the experiments. However, it was noted that the first measurement of each experimental campaign typically required more time for flame stabilization. This might suggest that surface adsorption occurs in the tube upstream of the burner until the surfaces become saturated with ammonia.

As for the second concern, color changes of the burner plate surface were observed after long-term operation with NH_3 , indicating possible surface adsorption. However, no signs of unexpected flame color or instability were detected. The flame remained stable, and the repeatability of measurements confirmed that the results were not affected by interactions between NH_3 and the brass components. These conclusions are consistent with previous studies involving ammonia in flat flame burners made of brass, which also investigated flame structure [57] and LBV [58].

4 Modeling method

This section discusses the modeling approaches. All modeling work was performed in ANSYS Chemkin-Pro software (<https://www.ansys.com>), which is designed to simulate the conditions necessary for analyzing combustion properties of interest.

4.1 Modeling for fundamental combustion experiments

4.1.1 Laminar burning velocity

4.1.1.1 *Module basics*

Laminar burning velocities are calculated using the Premix Laminar Flame Speed module of the Chemkin-Pro software. This module assumes a freely propagating adiabatic, premixed, stretch-free flame. In the flame coordinate system, the flame speed is defined as the inlet velocity (velocity of unburned gas moving toward the flame) that allows the flame to stay in a fixed location. The module provides one-dimensional outputs as a function of the distance. To set up the calculation, the compositions of the fresh gas mixture, the unburned gas temperature, and the pressure should be specified.

4.1.1.2 *Grid properties*

The simulation domain needs to extend over a distance that includes the entire reaction zone of the flame, i.e., until the temperature reaches a plateau. To ensure accurate resolution of steep gradients, Adaptive Grid Control was applied in the study based on Solution Gradients (GRAD) and Solution Curvature (CURV). The initial simulations are done on a very coarse mesh that may have as few as five or six points. After obtaining a solution on the coarse mesh, new mesh points are added in regions where the solution or its gradients change rapidly. GRAD refines the mesh in regions where the first derivative (rate of change) of solution variables exceeds a threshold. CURV refines the mesh based on the second derivative (the rate of change of gradient), capturing rapid variations in gradients to be less than another threshold. Typically, in this study, GRAD and CURV parameters were set to 0.02 and 0.05, respectively. These settings yield around 800 grid points over a 3 cm domain, ensuring grid-independent solutions.

4.1.1.3 *Thermal diffusion and transport options*

Simulations in this thesis considered thermal diffusion options. Thermal diffusion, also called the Soret effect, controls the mass flux through the temperature gradient of the flame. Thermal diffusion most strongly affects the diffusion of light species, such as hydrogen.

Simulations were also often run with the Multicomponent Transport option, which is highly recommended to improve accuracy. Multicomponent Transport accounts for the diffusion of a given species relative to each individual species through the flame, in contrast to the Mixture-averaged Transport option, where a species' individual diffusion is related to the bulk of the gas. However, the Multicomponent Transport option is usually computationally slower and harder to converge, which is often a problem for heavier fuels. For example, in Paper I, the Mixture-averaged Transport option was used for simulations of pyrrole flames, although a test with our model showed that this option only brought 0.1%–2.1% differences to the LBV results compared to Multicomponent Transport.

4.1.1.4 *Radiation heat loss*

Standard flame speed simulations are typically conducted under adiabatic conditions; however, radiation heat loss must be considered for slow flames as it significantly impacts the laminar burning velocity (LBV) and flame structure [59]. In Chemkin-Pro, radiative heat losses from radiating species are accounted for using the optically thin media radiation model.

In our model, the Planck-mean absorption coefficients for species of CH₄, CO, CO₂, H₂O, N₂O, NH₃, and NO are taken from [59]. These absorption coefficients, expressed as polynomial functions of temperature, describe the total emission from the medium and are formatted to be compatible with Chemkin-Pro's thermodynamic data files. In this study, the option of "include radiation heat loss" was selected when simulating NH₃ flames, while it has a minor effect on LBV results (less than 0.25 cm/s). In Paper IV, where flame structure is included, there is also no significant effect on the temperature and speciation profiles. This could be attributed to the fact that the flame reactivity of these mixtures is higher than that of pure NH₃-air flames, making radiation losses less pronounced. Not all chemical kinetic models include radiative species and their absorption coefficients; therefore, gas radiation effects were only considered for models that incorporated this information.

4.1.2 **Flame structure**

Flame structure simulations were performed using the Premixed Laminar Burner-Stabilized Stagnation Flame model. This module is used to simulate laminar, premixed flames stabilized on a burner, with one inlet for the premixed blend of fuel

and oxidizer and another boundary as a wall. The conservation equations governing this module and the Premix Laminar Flame Speed module are the same, but the boundary conditions differ. For burner-stabilized flames, the inlet mass flow rate is constant, the temperature and mass fraction are specified at the inlet cold boundary, and vanishing gradients are imposed at another boundary.

In this module, the temperature profiles can be either provided as in the experiments or determined by the energy conversion equation. In the case of providing experimental profiles, only the species transport equations are solved. In Paper IV, where flame structure measurements were involved, simulations were defined as solving the gas energy equation. Then, the experimental temperature profiles were also used as validation targets for models. Thermal diffusion effect and mixture-averaged transport were considered. Boundary conditions such as stagnation plate temperature, simulation axial distance, and mixture inlet velocity were specified to match those in the experiments. Depending on the used detailed kinetic model and the corresponding stiffness of convergence, mesh refinement tolerances for the species profiles were set to 0.02–0.23 for the GRAD parameter and 0.02–0.23 for the CURV parameter. The final grid for the flame contained approximately 100–600 mesh points.

4.1.3 Other experiments

The Closed Homogeneous Batch Reactor module was used for simulations of shock tubes. The module has zero dimensions with no spatial coordinate; the predicted activity is given as a function of time. The batch reactor emulates the uniformly distributed reactants in a confined volume in experiments with conserved mass. Adiabatic conditions are assumed during the modeling. No input parameters for transport need to be employed.

In this thesis, shock tube simulations were performed assuming constant volume and solving the energy equation. Non-ideal boundary conditions were considered as specified in the literature. The ignition delay times are steady-state solutions, and the definition of ignition moments was consistent with those in the literature experiments. Shock tube speciation profiles are transient solutions; the simulation results over time evolution were compared with the experiments.

The Plug Flow Reactor module was used for simulations of plug flow reactors. In this module, it is assumed that there is no mixing in the axial (flow) direction but perfect mixing in the direction transverse to this. In this study, fixed gas temperature or the variation of temperature profiles over the distance was applied in the simulations to be consistent with the literature. Reactor diameter, axial distance, temperature, pressure, axial velocity or flow rates, and mixture compositions were obtained from the literature.

The Perfectly Stirred Reactor module was used for simulations of the jet-stirred reactor, which assumes fast mixing and a homogeneous system, having inlet and outlet ducts. Simulation inputs, including residence time, temperature, pressure, reactor volume, flow rates, and mixture compositions, were obtained from the literature. In the Plug Flow Reactor module and Perfectly Stirred Reactor module, the determination of composition and temperature fields is assumed to be kinetically limited. Transport is assumed to be infinitely fast within the section of gas considered, and the effects of transport properties can be neglected.

4.2 Chemical kinetic analyses

4.2.1 A-factor sensitivity analysis

The many reactions in a kinetic mechanism all affect the examined property to different extents. Both to gain further knowledge of chemistry and to identify possible targets for improvement, it is of interest to quantify the effect of individual reactions on the combustion process as a whole.

Sensitivity analysis is a useful tool for evaluating quantitatively how an individual reaction influences the predictions of a property from modeling. Specifically, Chemkin-pro provides “A-factor sensitivity analysis” where the sensitivity coefficients S are calculated by how the simulation results y_i (speciation, ignition delays, or laminar burning velocities) depend on the pre-exponential A factors (in the Arrhenius expression) from each reaction. Normalized sensitivity coefficients are used in Chemkin-pro, which are expressed in Logarithmic derivative:

$$s = \frac{\partial \ln(y_i)}{\partial \ln(A_i)} \quad (4-1)$$

For steady-state solutions, such as laminar burning velocity and ignition delay time, the sensitivity coefficients s are fixed values that represent the overall influence of the A factor on the parameter y . These coefficients were visualized in the thesis using bar plots, where the x-axis represents the sensitivity coefficients, and the y-axis lists the reactions. For transient solutions—such as speciation profiles from shock tubes, flow reactors, and jet-stirred reactors, which evolve over time, as well as flame structure profiles that vary with height above the burner, the sensitivity coefficients s change dynamically with time or distance. This indicates that the impact of a reaction on the parameter y varies throughout the reaction process. To illustrate these variations, line plots were used, with the x-axis representing time or distance and the y-axis showing the sensitivity coefficients.

4.2.2 Rate of production analysis

The amount of a species present during combustion is dependent on the rate at which it is produced and the rate at which it is consumed. Chemkin-pro provides the rate of production (ROP) analysis, providing values of a species' overall production rate, as well as the rate of production from each reaction. The ROP values are expressed in units of $\text{mole}/(\text{cm}^3 \cdot \text{s})$. A positive ROP value indicates that a species is being produced, while a negative value represents that it is consumed faster than it is generated. By observing the rate of production of a species over time or distance, information can be obtained about dominant reactions influencing its concentration. ROP analysis can also highlight differences in how various mechanisms predict reaction behavior, which is especially useful when a species has minimal reactions consuming or producing it. Thus, the ROP analyses can identify a limited number of reactions for examination, as used in paper IV for analyzing dominating N_2O -chemistry reactions affecting its concentration.

4.2.3 Reaction pathway analysis

Reaction path analysis is useful for tracing the combustion process from fuel to major products. It is beneficial to tell the differences in different mechanisms predicting paths, thus explaining the dominant chemistry difference and helping to highlight specific reactions for examination (used in Paper II), or to tell the reaction paths difference when experimental conditions change, thus understanding different combustion behavior (used in Paper V).

Reaction pathway analyses are based on rate of production (ROP) analysis. In this thesis, the arrows in the reaction pathways represent the dominant consumption reactions of a species, as determined by the ROP analysis; the numbers next to the arrows, expressed as percentages, were calculated by dividing the rate of consumption of a species through a specific reaction by its total rate of consumption. In laminar flames, the ROP values of a species by a reaction vary with distance above the burner; therefore, in my papers, these percentages were calculated by dividing the integrated rate of consumption values of a specific reaction by the total integrated rate of consumption.

5 Results

This chapter begins with a discussion of the overall results and then presents and analyzes key representative results from selected papers.

5.1 Survey

This work investigates the fundamental combustion characteristics of various nitrogen-containing fuel mixtures, using the data for model validations and improvements. Each individual study within follows a systematic methodology, which is summarized below to provide a cohesive overview:

- 1) Measurements: Fundamental combustion data of specific mixtures were measured using our lab's setups, filling in a knowledge gap. Each study focuses on different fuel components to explore different dominant nitrogen chemistries.
- 2) Model validations: The new data, along with relevant literature data, were used to validate both our group's model and other well-known models.
- 3) Kinetic analyses: Kinetic analysis tools were used to understand dominant chemistry. Well-performing models helped highlight dominant reactions, while underperforming ones indicated reactions for review.
- 4) Model refinement: The rate constants of the dominant reactions were selected from the literature, judging by the updated model performances on the fundamental combustion data. Recent high-level theoretical calculation results were often preferred.
- 5) Model re-validation: The updated kinetic model was re-evaluated against new and existing combustion data.

Table 5.1 summarizes the investigated mixtures, experimental conditions, and targets in each paper, along with literature-relevant combustion data used for model validation. The model from our group was iteratively updated across studies *I–V*, presented in chronological order to indicate the most recent version. Figure 5.1 shows the dominant reactions in each paper, highlighting variations in the dominant nitrogen chemistry.

Table 5.1. Investigated mixtures, experimental targets and conditions, and literature data for model validations.

Model validations.					
Paper	Mixtures	Experimental targets/conditions			Literature validation targets
		Targets	Conditions		
			T (K)	Φ	
I	C ₄ H ₅ N+air	LBV	338	0.6–1.3	Speciation profiles during C ₄ H ₅ N pyrolysis and oxidation in JSR; Ignition delay times of C ₄ H ₅ N+O ₂ +Ar mixtures in ST; Speciation profiles during C ₄ H ₅ N oxidation in PFR.
II	NH ₃ +O ₂ +(30–60%) Ar	LBV	298	0.4–1.5	Speciation profiles during NH ₃ pyrolysis in ST; NO profiles during NH ₃ oxidation in ST; NO profiles in H ₂ +CO+CO ₂ +air flames; Flame structure of NH ₃ +O ₂ +(H ₂)+Ar; Ignition delay times of NH ₃ +O ₂ +Ar in ST; LBV of NH ₃ +O ₂ +He or (Ar+He); Speciation profiles during oxidation of NH ₃ +O ₂ +Ar and NH ₃ +NO ₂ +O ₂ +N ₂ in JSRs; Speciation profiles of NH ₃ +NO ₂ in PFR.
III	NH ₃ +[(30–50%)O ₂ +balanced N ₂]	LBV	298–348	0.4–1.7	LBV data of NH ₃ +(O ₂ +N ₂) with O ₂ in oxidizer varies from 60 to 100%; LBV of (NH ₃ +H ₂)+air at both 1 atm and high pressures; LBV of NH ₃ +O ₂ +Ar; LBV of NH ₃ +air at high temperature; Ignition delay times of NH ₃ +O ₂ +(H ₂)+Ar in ST; Speciation profiles during NH ₃ pyrolysis in ST; N ₂ O time-history of NH ₃ +O ₂ +Ar in ST.
IV	NH ₃ +O ₂ +~83 %Ar	Flame structure	303	0.8–1.2	Flame structure of NH ₃ +O ₂ +Ar; LBV of (NH ₃ +H ₂)+air at 1 atm and high pressures; LBV of NH ₃ +O ₂ +Ar; LBV of NH ₃ +air at high temperature; Ignition delay times of NH ₃ +O ₂ +Ar in ST.
V	[(0–80%) NH ₃ +balanced CH ₃ NO ₂]+air	LBV	298	0.7–1.7	LBV of NH ₃ +(NO+N ₂).

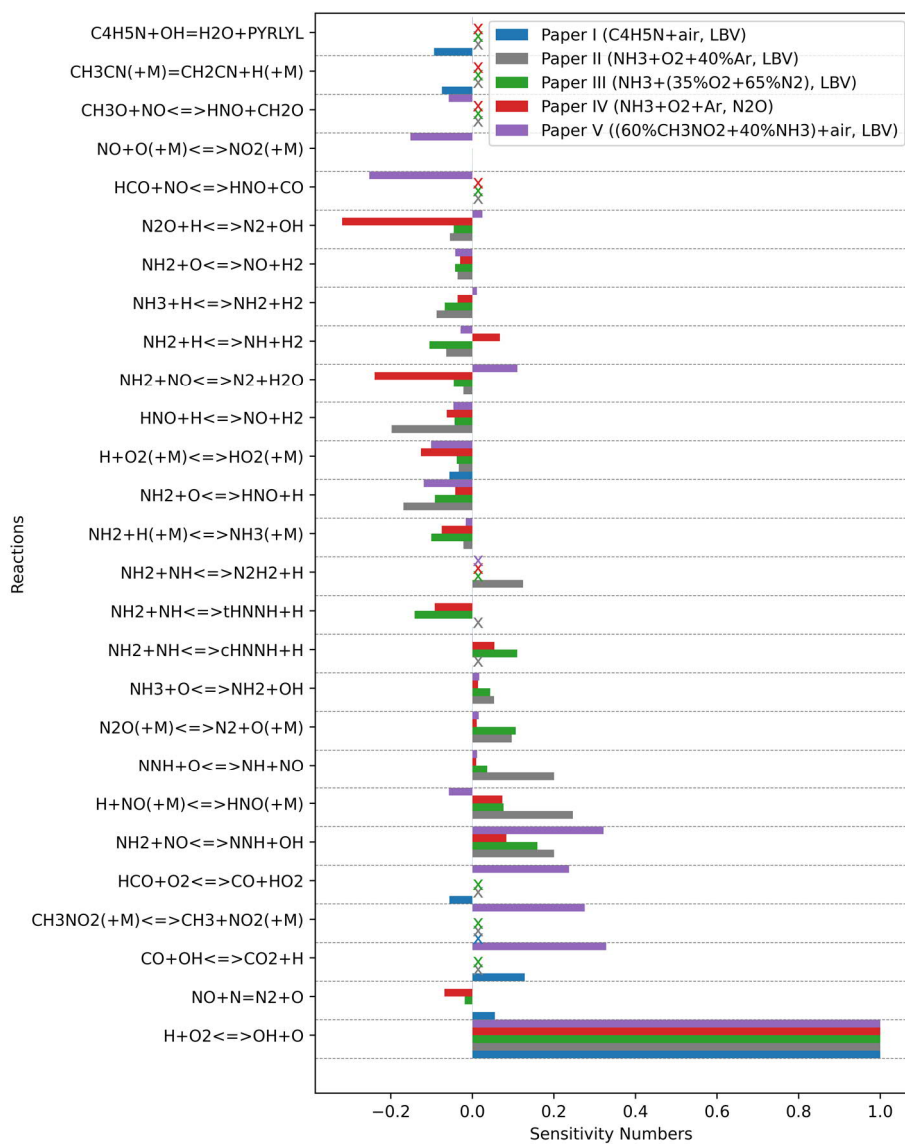


Figure 5.1 Dominant reactions in each paper. A specified gas mixture was selected for the comparison, and the simulations were performed using the updated kinetic model corresponding to that study. The sensitivity numbers represent the actual sensitivity coefficients normalized by the sensitivity coefficients of the reaction $H+O_2 = O+OH$ in each respective case. The crosses ("x") indicate that the corresponding reaction is not included in that version of the kinetic model.

5.2 NH₃+O₂+Ar mixtures

Most often, ammonia combustion is studied in air or other (O₂+N₂) mixtures with varying oxygen content due to their relevance to practical combustion scenarios. Although using argon (Ar) as a diluent instead of nitrogen (N₂) is less practical from an application perspective, it can elucidate specific ammonia flame chemistry that is vastly different from those of NH₃+O₂+N₂ mixtures. Ar's lower heat capacity compared to N₂ results in higher adiabatic flame temperature, allowing for the examination of ammonia chemistry at a higher temperature region. The different dominant atmosphere of Ar also provides a chance to scrutinize its third-body collisional efficiencies in reactions.

Many studies on the NH₃+O₂+Ar or NH₃+O₂+Helium (He) system have been carried out, including studies in shock tubes [26, 60], jet-stirred reactors [61, 62], flow reactor [62], and stabilized flames [63, 64]. However, LBV data of NH₃+O₂+Ar mixtures are rather scarce. There is insufficient knowledge of the kinetic model performance in predicting LBVs for NH₃+O₂+Ar mixtures.

Meanwhile, Osipova et al. [64] measured major and minor species profiles in NH₃+H₂+O₂+Ar flames at 4 and 6 atm using molecular beam mass-spectrometry and compared them with predictions of eight recently developed kinetic models. While the profiles of major species (NH₃, H₂, O₂, N₂, and H₂O) were well reproduced, model prediction performances for NO and N₂O profiles vary. Similar discrepancies were also observed by Osipova et al. [63] at atmospheric pressure in NH₃+O₂+Ar and NH₃+H₂+O₂+Ar flames. It is noticed that the experimental uncertainty for NO_x measurements in the work of Osipova et al. [63, 64] was $\pm 50\%$ and emphasized the need for further studies of nitrogen chemistry in ammonia flames.

To address these gaps, LBVs and flame structure, including NO_x measurements for NH₃+O₂+Ar mixtures, were studied in Papers *II* and *IV*.

5.2.1 LBV results and modeling

In Paper *II*, laminar burning velocities of (NH₃+O₂+Ar) mixtures were studied using the heat flux method, at an initial temperature of 298 K and atmospheric pressure over an equivalence ratio range of 0.4–1.5. The Ar mole percentage in the mixture varied from 30 to 60 %. The kinetic model from our research group and other popular literature kinetic models were validated.

Figure 5.2 compares parts of the LBV results with the model predictions, revealing significant variations between the models. The “present model” is the model updated in Paper *II*, which incorporated improvements to the most recent nitrogen

chemistry in the base model, referred to as “2021 Han” [35], also from our group. Both models perform well in capturing LBVs across the tested conditions.

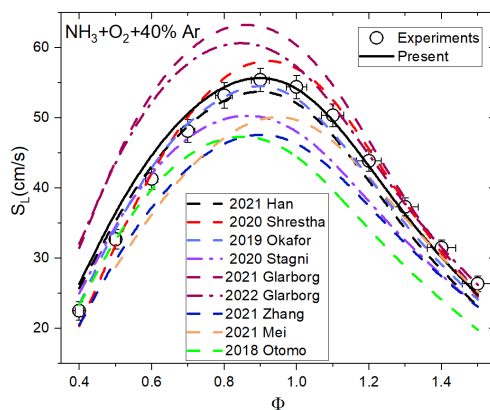


Figure 5.2 Comparison of the present model in Paper II (solid line) and literature models for LBV of the $\text{NH}_3+\text{O}_2+\text{Ar}$ flames.

The developments of the present model were based on comparisons with other literature pyrolysis and oxidation data from the $\text{NH}_3(+\text{O}_2)+\text{Ar}$ system. Figure 5.3 shows the experimental and computational NH_3 time histories for the NH_3+Ar mixture at low (2096 K, blue), medium (2258 K, grey), and high temperatures (2487 K, red). The experimental data are from Alturaifi et al. [26]. As one can see, the 2021 Han model over-predicts the consumption rate of NH_3 .

Figure 5.4 shows the seven most sensitive reactions and sensitivity coefficients for NH_3 concentration at 2400 K and 1 atm, over the whole reaction time reported in Figure 5.3 (0–2500 μs). The plot in the early stage (< 100 μs) is enlarged, as shown in the inset. As can be seen, $\text{NH}_2+\text{H}(+\text{M})=\text{NH}_3(+\text{M})$, denoted in the black line, is the dominating reaction for NH_3 consumption, and at the early stage, it is the only reaction that governs NH_3 consumption.

Therefore, reviews were then carried out on the rate constants of reaction $\text{NH}_2+\text{H}(+\text{M})=\text{NH}_3(+\text{M})$. It was found that Glarborg et al. [65] calculated the relative temperature-dependent collision efficiencies of N_2 , Ar , O_2 , and NH_3 at three temperatures, i.e., 300 K, 1000 K, and 2000 K; their suggested collisional efficiencies at 300 K are $\text{N}_2:\text{Ar}:\text{O}_2:\text{NH}_3=1:0.32:0.5:4.39$. While in the 2021 Han model, the collisional efficiency of NH_3 was not included. Therefore, in Paper II, the third body collision efficiencies at 300 K from Glarborg et al. [65] have been adopted and tested using NH_3 pyrolysis data from Alturaifi et al. [26], as shown in

Figure 5.3. Following the update, the NH_3 profiles were accurately captured by the present model, demonstrating good agreement with the experimental data in Figure 5.3.

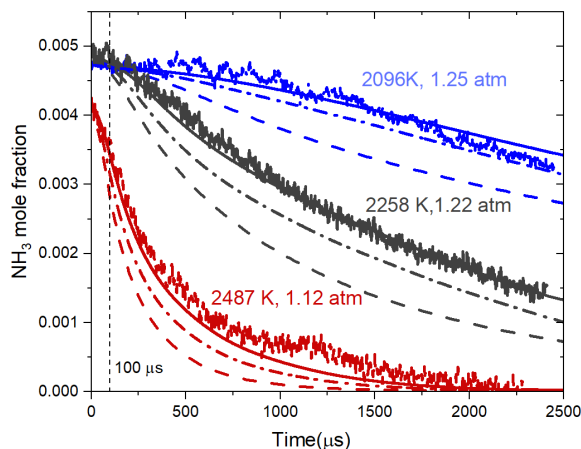


Figure 5.3 Experiments [26] and modeling (smooth lines) results for NH_3 speciation profile in a mixture of 0.5% NH_3 in Ar. Solid lines: the present model in Paper II using collision efficiencies at 300 K from Glarborg et al. [65]; dash-dot lines: the present model using collision efficiencies at 2000 K from Glarborg et al. [65]; dashed lines: the 2021 Han model.

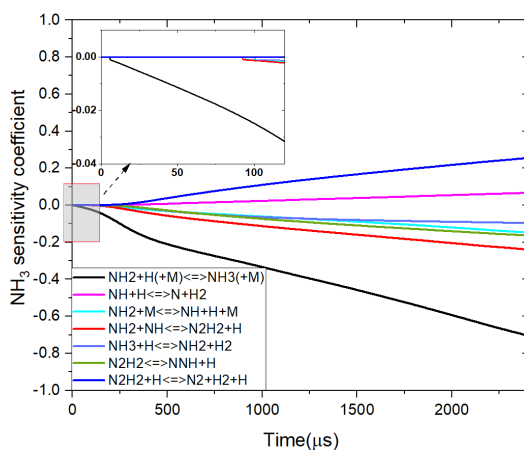


Figure 5.4 NH_3 sensitivity coefficients during NH_3 pyrolysis in a mixture of 0.5% NH_3 in balanced Ar, calculated using the present model in Paper II at 2400 K and 1 atm. The early stage (0–100 μs) is enlarged in the inset.

Using the same methodology, two additional reactions were revisited: the rate constant of $\text{NH}_2 + \text{O} = \text{HNO} + \text{H}$ have been selected using literature shock tube speciation data [66] and flame structure data [63, 64] of $\text{NH}_3 + \text{O}_2 + (\text{H}_2) + \text{Ar}$ mixtures; The rate constant of $\text{NNH} + \text{O} = \text{NO} + \text{NH}$ were selected among the literature expressions [67-69] with the help of literature flame structure data of $\text{H}_2 + \text{CO} + \text{CO}_2 + \text{air}$ mixtures [67]. Details can be found in Paper II.

5.2.2 Flame structure results and modeling

In Paper IV, new flame structure data of atmospheric $\text{NH}_3 + \text{O}_2 + \text{Ar}$ flames were studied at three equivalence ratios ($\Phi = 0.8, 1.0, 1.2$), at an initial temperature of 303 K, above a porous-plug McKenna burner using Raman spectroscopy. This technique offers the possibility to perform non-intrusive measurements in situ.

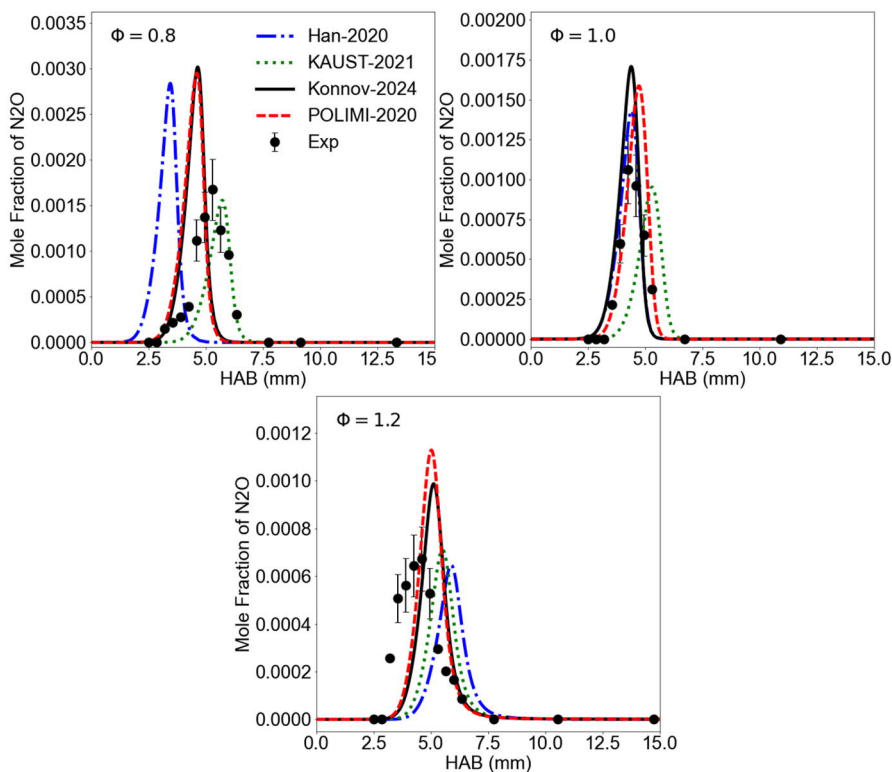


Figure 5.5 N_2O change with HAB. Experimental values (circles) compared with predictions of four kinetic models (lines): the model updated in Paper IV (the “Konnov-2024” model), and three literature models [70-72].

NO and N₂O spatial profiles were measured, with detection limits of 600 and 500 ppm, respectively, in addition to the determination of O₂, N₂, NH₃, H₂O, H₂, and temperature. A detailed kinetic model from our group was validated and modified, focusing on N₂O chemistry (the “Konnov-2024” model). Three literature models [70-72] were also validated, as they were claimed in a review paper [73] to be the best-performing models for data of NH₃/H₂ fuel mixtures.

Figure 5.5 presents N₂O mole fraction profiles in the three flames plotted against the height above the burner surface (HAB). The agreement with the models varies across the cases, for both flame position and maximum concentration. The KAUST-2021 [71] model captures the peak concentration of N₂O best.

To investigate the reason for different N₂O predictions, kinetic analyses were conducted using the Konnov-2024 and KAUST-2021 models. Rate-of-production (ROP) analysis at stoichiometric conditions reveals that in both models, the reaction $\text{NO} + \text{NH} = \text{N}_2\text{O} + \text{H}$ (or its equivalent reverse reaction $\text{N}_2\text{O} + \text{H} = \text{NO} + \text{NH}$) is the sole pathway for N₂O formation within the reaction zone. Once formed, N₂O is predominantly consumed through the reaction $\text{N}_2\text{O} + \text{H} = \text{N}_2 + \text{OH}$ and the third-body dissociation reaction $\text{N}_2\text{O} (+\text{M}) = \text{N}_2 + \text{O} (+\text{M})$.

Nevertheless, the Konnov-2024 and KAUST-2021 models utilize different sources for the rate constant of the N₂O+H branches ($\text{N}_2\text{O} + \text{H} = \text{NO} + \text{NH}$ and $\text{N}_2\text{O} + \text{H} = \text{N}_2 + \text{OH}$) and the reaction $\text{N}_2\text{O} (+\text{M}) = \text{N}_2 + \text{O} (+\text{M})$. Further refinements to the Konnov-2024 model regarding N₂O predictions will be made, taking into account the most recent analysis of Glarborg et al. [74], focusing on N₂O+H reactions.

5.3 NH₃+O₂+N₂ mixtures

In Paper III, data inconsistency between literature LBV measurements of oxygen-enriched NH₃+(O₂+N₂) was highlighted. Figure 5.6 shows the LBV temperature dependence factor, which was used as an indicator of the data consistency between different studies. As can be seen, the power exponents α decreases with the equivalence ratio varying from 0.8 to 1.1, then increases as the equivalence ratio continues to rise from 1.1 to 1.4. This observed trend aligns with earlier experimental and modeling analysis in NH₃+air flames by Han et al. [75]. However, this evolution between α and Φ is different when processing the experimental data from Shrestha et al. [76], where α values scatter hectically along Φ . The simulations from the model they developed [76] are also beyond the error bars of their own experiments. The α values from Hamadi et al. [77] agree with those of the present study within the uncertainty range. This inconsistency addresses the necessity for a revision of detailed kinetic models and the inherent challenges in obtaining accurate LBV at different institutions.

It is noteworthy that Hamadi et al. [77] found that the discrepancy with Shrestha et al. [76] stemmed only from the flame stretch correction procedure used in determining the LBV. When both studies used the same flame radius domain, they obtained consistent LBV data. Hamadi et al. [77] emphasized that the domain size must be sufficiently large to ensure reliable LBV determination.

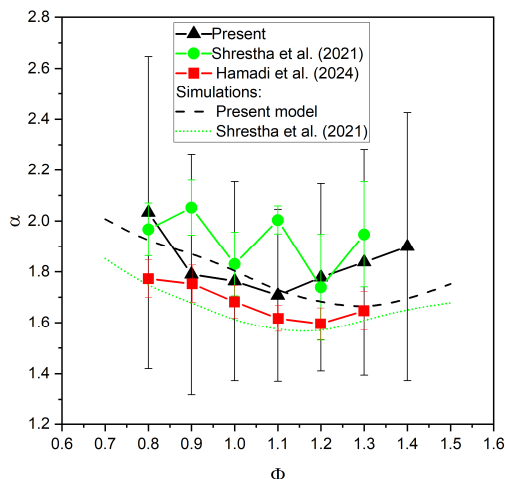


Figure 5.6 Experimental (line + symbols) and simulated (lines) temperature dependence factors for $\text{NH}_3 + (30\% \text{O}_2 + 70\% \text{N}_2)$ flames. Experiments are from the present study, Shrestha et al. [76] and Hamadi et al. [77].

Paper *III* introduced further updates after Paper *II*. The collisional efficiencies for $\text{NH}_2 + \text{H} (+\text{M}) = \text{NH}_3 (+\text{M})$ were revisited by us again using recent calculations from Jasper's [78], which indicated that both H_2O and NH_3 have even higher significant collisional efficiency than the ones considered in Paper *II*. The rate constant of $\text{NH}_2 + \text{O} = \text{HNO} + \text{H}$ was also updated again with other product channels ($\text{NH} + \text{OH}$ and $\text{NO} + \text{H}_2$) based on recent calculations of Klippenstein et al. [79]. Although their results for $\text{NH}_2 + \text{O} = \text{HNO} + \text{H}$ agree well with the ones adopted in Paper *II*, i.e., the results from Miller et al. [80], as shown in Figure 5.7.

The updated model in Paper *III* performs well in predicting LBV of the $\text{NH}_3 + \text{O}_2 + \text{N}_2$ flames, as well as $\text{NH}_3 + \text{H}_2$, $\text{NH}_3 + \text{O}_2 + \text{Ar}$, and high-temperature $\text{NH}_3 + \text{air}$ flames.

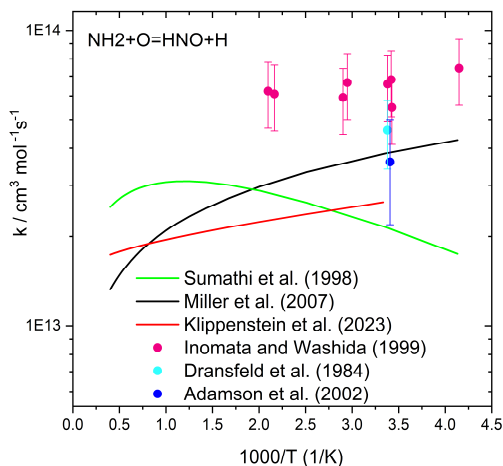


Figure 5.7 Rate constants of $\text{NH}_2+\text{O}=\text{HNO}+\text{H}$. Paper II adopted the results from Miller et al. [80], and Paper III further adopted it as the new calculation results from Klippenstein et al. [79]. Other reference sources can be found in Paper II.

5.4 $\text{CH}_3\text{NO}_2+\text{NH}_3$ +air mixtures

Nitromethane (CH_3NO_2) is a green monopropellant, since it has low toxicity and relative stability compared with hydrazine and hydrazine-based propellants [81], racing fuel [82], and gasoline fuel additive [83]. It is the simplest organic nitro compound. Moreover, nitromethane is also a nitric oxide (NO) precursor; thus, burning CH_3NO_2 with NH_3 could offer the opportunity to study the interactions between NO_x and NH_3 . So far, only Zheng et al. [84] have investigated the interactions between NH_3 and CH_3NO_2 in the shock tube.

In Paper V, the laminar burning velocities of $\text{NH}_3+\text{CH}_3\text{NO}_2$ blends burning in the air have been measured using the heat flux method. The NH_3 mole fraction in the fuel blends varies from 0% to 70%, covering fuel-lean to fuel-rich conditions, at a fixed initial temperature of 338 K and 1 atm. Figure 5.8 shows part of the LBV results from Paper V, comparing three kinetic models: the “present model”, the model of Mathieu et al. [85], and the model of Shrestha et al. [86]. The “present model” is the model from our research group and was updated in Paper V. In this model, CH_3NO_2 modeling was updated with the introduction of reactions of CH_3NO_2 , CH_2NO_2 , methyl-nitrite (CH_3ONO), and hydrogen isocyanide (HNC), following the suggestions of Glarborg et al. [87].

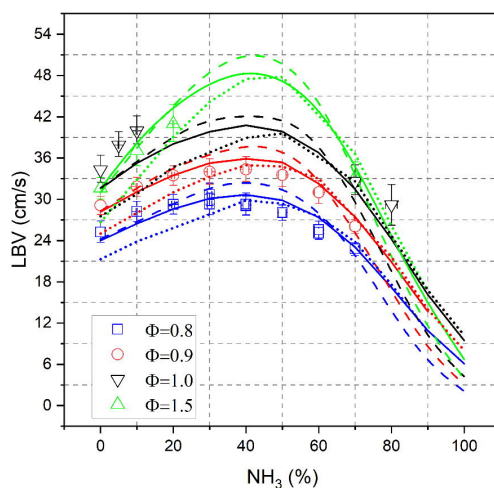


Figure 5.8 Experimental (symbols) and simulated (lines) LBV of $(\text{CH}_3\text{NO}_2+\text{NH}_3)+\text{air}$ mixtures with various $\text{NH}_3\%$ in the fuel, at $\Phi = 0.8, 0.9, 1.0$, and 1.5 . Solid lines: the present model, dashed lines: the model of Mathieu et al. [85], dotted lines: the model of Shrestha et al. [86].

In Figure 5.8, the LBV of the mixture follows a parabolic-like trend with respect to $\text{NH}_3\%$. As $\text{NH}_3\%$ in the fuel blend increases, the LBV initially rises, reaching a maximum at around 40% NH_3 , and then decreases. This trend is consistent across different equivalence ratios $\Phi = 0.8, 0.9, 1.0$, and 1.5 . Both the “present model” and the model of Mathieu et al. [85] predict the available LBV data well. The Shrestha model [86] under-predicts the LBV of $(\text{CH}_3\text{NO}_2+\text{NH}_3)+\text{air}$ mixtures when $\text{NH}_3\%$ is below approximately 30% but performs better as $\text{NH}_3\%$ increases.

Generally speaking, $\text{CH}_3\text{NO}_2+\text{NH}_3$ mixtures constitute an unexpected and unique case when ammonia addition increases the burning velocity of a fuel blend. This behavior contradicts all previously studied mixtures with H_2 , hydrocarbons, or biofuels. The only exception to this behavior was demonstrated and discussed by Wang et al. [52]. The authors found in the experimental study and modeling that for the fuel blend of NH_3+CO , a small addition of ammonia increases LBV. This is not surprising since it is well known that dry $\text{CO}+\text{air}$ mixtures have very low LBV, while adding hydrogen in any form, even as H_2O , increases it by activating the chain-branching reaction $\text{H}+\text{O}_2=\text{OH}+\text{O}$.

Sensitivity analysis of LBV was performed using the “present model” under stoichiometric conditions, with 0%, 10%, 40%, and 80% NH_3 in the fuel blends (Figure 5.9). The chain branching reaction $\text{H}+\text{O}_2=\text{OH}+\text{H}$ is always the most sensitive reaction in all fuel blends. For $\text{CH}_3\text{NO}_2+\text{air}$ mixtures, reactions involving

species of CO, HCO, and CH₃O are crucial. Reaction $\text{CO}+\text{OH}=\text{CO}_2+\text{H}$ plays a dominant LBV-promoting role, followed by H radical producing reactions $\text{HCO}(\text{+M})=\text{H}+\text{CO}(\text{+M})$ and $\text{CH}_3\text{O}(\text{+M})=\text{CH}_2\text{O}+\text{H}(\text{+M})$, and CO producing reaction $\text{HCO}+\text{O}_2=\text{CO}+\text{HO}_2$. OH producing reaction $\text{NO}+\text{HO}_2=\text{NO}_2+\text{OH}$ is also reactivity-promoting, followed by NO producing reaction $\text{CH}_3+\text{NO}_2=\text{CH}_3\text{O}+\text{NO}$. Conversely, reactions consuming NO, such as $\text{HCO}+\text{NO}=\text{HNO}+\text{CO}$, $\text{NO}+\text{O}(\text{+M})=\text{NO}_2(\text{+M})$ and $\text{CH}_3\text{O}+\text{NO}=\text{HNO}+\text{CH}_2\text{O}$, exhibit inhibitory effects on flame reactivity, since they compete with $\text{NO}+\text{HO}_2=\text{NO}_2+\text{OH}$. The bond scission reaction $\text{CH}_3\text{NO}_2(\text{+M})=\text{CH}_3+\text{NO}_2(\text{+M})$ produces CH₃ and NO₂, which act as key fuel and oxidizer intermediates, thus also showing strong sensitivity.

As NH₃% increases, NH₃-related oxidation chemistry becomes increasingly significant, ultimately dominating the overall reactivity at 80% NH₃, as shown by the green bars in Figure 5.9. Interestingly, even with only 10% NH₃ in the fuel, the sensitivity coefficient of $\text{NH}_2+\text{NO}=\text{NNH}+\text{OH}$ becomes significant. Furthermore, the reaction $\text{NH}_2+\text{NO}=\text{N}_2+\text{H}_2\text{O}$, typically a reactivity-inhibiting reaction in NH₃ flames, enhances flame reactivity in CH₃NO₂+NH₃ flames when NH₃% is below 80%. Generally speaking, it was suggested that the addition of ammonia to the fuel blend converts part of the NO formed in nitromethane oxidation, producing N₂ that, in turn, leads to supplementary heat release.

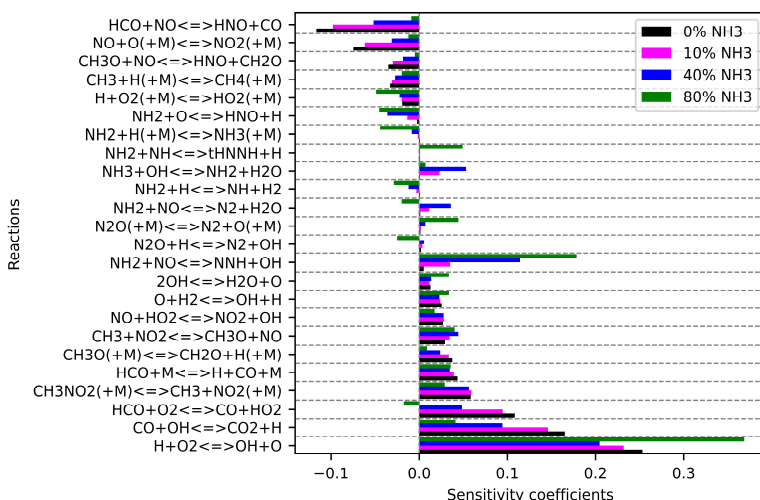


Figure 5.9 Sensitivity spectra for $(\text{CH}_3\text{NO}_2+\text{NH}_3)+\text{air}$ flames, at stoichiometric conditions, 338 K, 1 atm.

Further flux analysis (Figure 5.10) confirmed that interactions between NH_3 and CH_3NO_2 occur primarily through reactions of NH_2 radicals with NO , which is directly produced from CH_3NO_2 .

In Figure 5.10, with 40% NH_3 in the fuel blend, as illustrated by the blue pathways and numbers, the NH_3 primary oxidation pathway appears to be: $\text{NH}_3 \rightarrow \text{NH}_2 \rightarrow \text{NNH} \rightarrow \text{N}_2$. Nearly all NH_3 converts to NH_2 , which will react directly with NO that is produced from CH_3NO_2 through reactions $\text{NO} + \text{NH}_2 = \text{NNH} + \text{OH}$ (18%) and $\text{NH}_2 + \text{NO} = \text{N}_2 + \text{H}_2\text{O}$ (23%). Consequently, NO consumption pathways participated in $\text{CH}_3\text{O} \rightarrow \text{CH}_2\text{O}$ and $\text{HCO} \rightarrow \text{CO}$ in the neat nitromethane flame diminished to 11% and 14%, respectively. These pathways, which inhibit flame reactivity, become less prominent, as manifested in Figure 5.9.

At 80% NH_3 , more NH_2 radicals convert into NH (31%), as NO from CH_3NO_2 decreases, reducing participation in $\text{NH}_2 + \text{NO} = \text{NNH} + \text{OH}$ (10%) and $\text{NH}_2 + \text{NO} = \text{N}_2 + \text{H}_2\text{O}$ (12%), as illustrated by the green numbers. Reactions in NH_3 chemistry dominate, and the lower reactivity of NH_3 reduces LBV for blends with further increasing $\text{NH}_3\%$. More details are in Paper V.

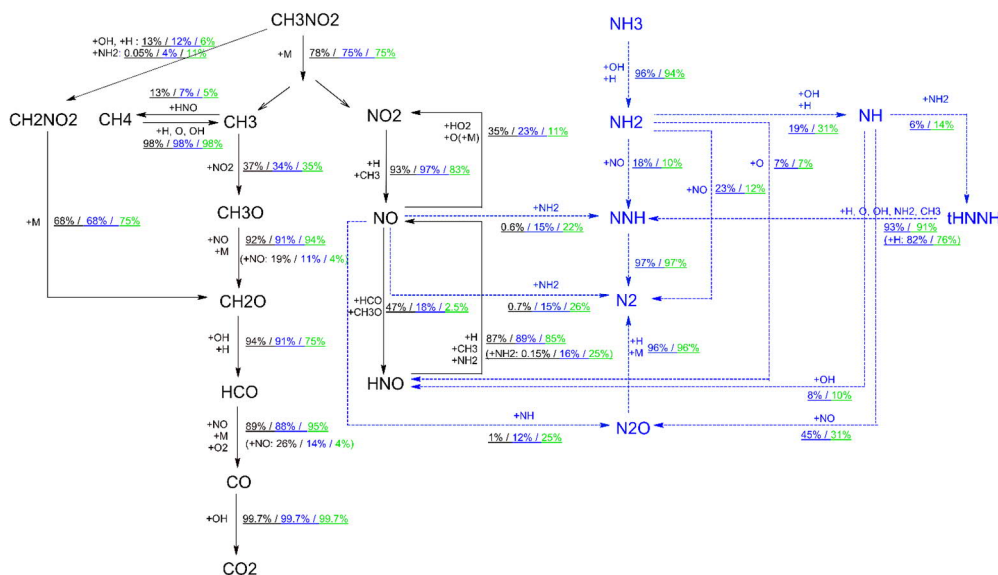


Figure 5.10 Species reaction pathways at stoichiometric condition. Black numbers: 0% NH_3 ; Blue numbers: 40% NH_3 ; Green numbers: 80% NH_3 .

6 Summary and outlook

6.1 Summary

Ammonia (NH_3) has attracted considerable attention as a potential carbon-free alternative fuel. To enable low-emission, high-efficiency combustion, it is essential to develop accurate chemical kinetic models that describe ammonia's combustion behavior at the molecular level. In addition to ammonia, other nitrogen-containing compounds are commonly found in conventional and bio-derived fuels, which can introduce fuel-bound NO_x emissions. Therefore, building reliable chemical kinetic models for these critical nitrogen-containing fuels is also of great importance.

To ensure the accuracy of such models, validation through fundamental combustion experiments is necessary. These experiments isolate chemical kinetics by minimizing the influence of complex physical phenomena. They also offer valuable insights into the fundamental combustion characteristics of fuels of interest.

This study presents five separate investigations on fundamental combustion experiments on nitrogen-containing fuels, with a primary focus on laminar burning velocity (LBV) and additional investigation into flame structure. LBV reflects the global reactivity of a fuel-air mixture, while flame structure reveals micro-scale combustion characteristics, serving as more stringent validation targets. The heat flux method was employed for LBV measurements, and was introduced in the study. Measurements of flame structure were conducted by A. Zubairova and are presented in her doctoral thesis.

In each investigation, the fuel mixture components were varied, enabling the examination of distinct dominant chemistry. Throughout these studies, the chemical kinetic model developed by our group was iteratively updated. In the first study, pyrrole ($\text{C}_4\text{H}_5\text{N}$)—the simplest five-membered nitrogen-containing aromatic compound—was selected as a model fuel to explore fuel-bound nitrogen combustion chemistry. LBVs of pyrrole+air mixtures were measured, and detailed reaction mechanisms for pyrrole combustion were updated accordingly.

Ammonia was investigated in mixtures with various diluents, dilution ratios, and fuel blends, starting with LBV measurements in $\text{NH}_3+\text{O}_2+\text{Ar}$ mixtures. Nine published kinetic models were evaluated, and three key reactions, $\text{NH}_2+\text{H}(+\text{M})=\text{NH}_3(+\text{M})$, $\text{NNH}+\text{O}=\text{NH}+\text{NO}$, and $\text{NH}_2+\text{O}=\text{HNO}+\text{H}$, were revised. Further studies on oxygen-enriched ammonia flames revealed discrepancies with

existing literature data, prompting updates to reactions involving N_2H_2 , NH_2O , and third-body efficiencies of NH_3 . These refinements significantly improved model predictions for $\text{NH}_3+\text{H}_2+\text{air}$ and NH_3+air flames at high temperatures.

Raman spectroscopy was employed to non-intrusively detect NO and N_2O in ammonia flames, providing valuable datasets for model validation. In the final investigation, ammonia was blended with nitromethane (CH_3NO_2), revealing a non-monotonic effect of NH_3 addition on flame reactivity. Kinetic analyses attributed this behavior to the effectiveness of the interactions between NH_2 and NO .

In summary, this work delivers fundamental combustion data for key nitrogen-containing fuels and supports the ongoing validation and improvement of nitrogen chemistry within chemical kinetic models.

6.2 Outlook

For ammonia chemistry, continued efforts should focus on refining N_2O kinetics to further enhance the accuracy of our model, particularly in light of a recent theoretical study [74] that investigated the $\text{N}_2\text{O}+\text{H}$ system. Our ongoing investigations into the laminar burning velocities of $\text{NH}_3+\text{N}_2\text{O}+\text{H}_2\text{O}$ mixtures might offer a valuable opportunity to examine key reactions, where reactions in N_2O chemistry are highly sensitive. Additionally, further modeling work could be directed toward other important nitrogen-containing fuels, which calls for reviews of the current progress for the species of interest.

Furthermore, it would be beneficial to conduct a more comprehensive validation of the latest kinetic models from our group. Achieving this would require large-scale data collection and extensive simulations. Given the complexity of this task, leveraging automated model validation tools, such as the Optima++ software from Eötvös Loránd University, could simplify the process.

In my view, it would greatly benefit the combustion community to establish a publicly accessible system that enables researchers to update their published experimental data and rate constants, thereby facilitating peer review and advancing progress toward an approximately unified model. The use of additional automated model validation software is also crucial, as it not only reduces the time and effort required for repeated simulations but also minimizes random inaccuracies by systematically recording standardized input data files. This is particularly useful when certain critical details are missing from published experimental work. In such cases, researchers often rely on personal communication to obtain this information, and this issue could be resolved once and for all through proper recording of standardized input data files.

Acknowledgements

Now, my wonderful, unique, and full of taste journey as a PhD student has come to an end. Looking back at the four years of memories I had in the Division of Combustion Physics, where I've grown from age 24 to now, I feel deeply proud to spend these years in this special place, and I would like to give my deep gratitude to the people I met during the journey.

I would first like to thank my main supervisor, Alexander Konnov, a very reliable boss, researcher and teacher. Your remarkable dedication and passion for science are impressive, and I hope I can carry on this attitude to my future work as well. Thank you for always being open to my questions and patiently explaining them; and thank you for joining every of my Tuesday meeting presentations even when you were traveling and joined Thursday Fika sessions I hosted!

Then, I would like to thank my co-supervisor, Marco, who was with me only during my first year but taught me so much in that time. You are the most fun, diligent, knowledgeable, and hands-on boss that one could ever have!

I would like to thank Marcus, Per-Erik, and Joakim, for creating and managing this fantastic division. A place where people feel free to talk and share their minds and treat each other with respect.

Christian and Alsu, I enjoyed working with you very much! Christian, thank you for being so helpful, not just with the research, but also with all the little miscellaneous things that come up, we all say that the division wouldn't run without you. Alsu, thank you for being such a reliable, calm, relaxed and unique friend to me. I enjoyed the relaxing time with you very much to be away from the public.

Teacher Hu, Qianjin, Zhaomin, and Jibiao, although you only stayed (or about to stay) one year here as exchange researchers, I enjoyed your company in the lab and our spontaneous combustion discussions. You guys also brought much laughter to my life in Sweden! Vladimir, I appreciated all the discussions we had about the heat flux burner, or more accurately, me asking the "Bible creator" for guidance. I also truly appreciated your nice words, always complimenting and encouraging my work. Gianluca, you are so unique, and I enjoyed every meet-up with you.

Cecilia, Minna, Ida, Elizabeth, Charlotta, Sven-Inge and Emelie, thank you for all your help in keeping the division's economy and other activities organized. Your support allows us to stay focused on our headache and never-ending problems. Igor,

thank you for being such a helpful and professional technician and I also enjoyed your unexpected humor. Elizabeth, also thank you for bringing me to the most delicious tacos. Edouard, Mikkel, Adam, Elna, Frederik, Mattias, Cuong, Anna-lena, Moa, Arman, Li, Elias, Johan, Andreas, Birgitta and Erik, I like all the inspiring and smart thoughts you brought up during meetings and lunches.

Megha, Jan-peter, David, Meena, Lisa, Meng, Saga, Aravind, and Martin, although we did not have collaborations together, thank you not only for being the inspiring and loving colleagues that one can discuss with during lunches, but also the most awesome friends that could create wonderful memories with. Megha, also thank you for all the mental support that you've given and laughter you brought, and my time and place is also open for you if you ever become a PhD student mental refugee. Frej and Jacobo, thank you for being so relaxed officemates! I felt like I was at home when I closed the office door. Pranjali, Jefry, Vassily, Sebastian, Jonas, August, Henrik, and Haryo, thank you for always making the lunch table such a fun place. Zhiyong, Jinguo, and Kailun, you are all so warm and full of great advice, I enjoyed the memories we had. Xin, Qingshuang, and Yupan, thank you for being the greatest seniors and I truly appreciate all your warm and generous help throughout my journey. Qi Qi, Can, Xiaomin, Weitian, and Xu Jiang, although we haven't spent a long time together, I enjoyed the memories we've shared.

Yue, thank you for being such a wonderful friend and accompanied me for the whole journey, I've learned so much from you. Miaoxin and Shuo, thank you for inviting me to the Zumba class and sharing your energy with me, I always enjoy your company. Miss. Yuheng Shang, my roommate since university. Oh no, here you come again! But I feel so lucky to have you here in Europe and to share vacation moments with you. Qiuqiu, thank you for all the caring and happiness you brought. Blanca, Victoria, and Dorain, thank you for making my first-year corridor life so full of love and fun.

I would like to give my appreciation to my family. Thank you to my parents for showing your love and support by preparing and sending me your handmade food every year, and for always doing your best to make my journey back home as enjoyable as possible. Thanks to my siblings, I've never felt alone with you by my side. Thank you for always caring for my happiness when I am away, and for picking me up at the airport and helping with my luggage when I get home. 爸妈, 谢谢你们多年来对我学业的支持, 谢谢你们不远万里也要为我寄好吃的。弟弟妹妹们, 陈玉蝶, 陈俊鑫, 谢谢你们的关心和照顾。除了美食, 每年回家最期待的就是和你们见面!

Ruikun, thank you for being such a happy, loving, and understanding partner. No matter what kind of day I've had, I know I'll end it with laughter and relaxation when I'm with you. You make my life in Sweden beyond 100% happiness.

References

- [1] H.J. Curran, Developing detailed chemical kinetic mechanisms for fuel combustion, *Proc. Combust. Inst.* 37 (2019) 57-81.
- [2] United Nations, The Paris Agreement, 2015.
http://unfccc.int/files/essential_background/convention/application/pdf/english_paris_agreement.pdf (accessed March 2025).
- [3] EDGAR (Emissions Database for Global Atmospheric Research), GHG emissions of all world countries, 2024. https://edgar.jrc.ec.europa.eu/report_2024 (accessed March 2025).
- [4] A. Valera-Medina, H. Xiao, M. Owen-Jones, W.I.F. David, P.J. Bowen, Ammonia for power, *Prog. Energy Combust. Sci.* 69 (2018) 63-102.
- [5] G.W. Crabtree, M.S. Dresselhaus, M.V. Buchanan, The hydrogen economy, *Physics Today* 57 (2004) 39-44.
- [6] Y. Kojima, Hydrogen storage materials for hydrogen and energy carriers, *Int. J. Hydrog. Energy* 44 (2019) 18179-18192.
- [7] V. Negro, M. Noussan, D. Chiamonti, The potential role of ammonia for hydrogen storage and transport: A critical review of challenges and opportunities, *Energies* 16 (2023) 6192.
- [8] O. Elishav, B. Mosevitzky Lis, E.M. Miller, D.J. Arent, A. Valera-Medina, A. Grinberg Dana, G.E. Shter, G.S. Grader, Progress and Prospective of Nitrogen-Based Alternative Fuels, *Chem Rev* 120 (2020) 5352-5436.
- [9] H. Kobayashi, A. Hayakawa, K.D.Kunkuma A. Somarathne, Ekenechukwu C. Okafor, Science and technology of ammonia combustion, *Proc. Combust. Inst.* 37 (2019) 109-133.
- [10] R. Lan, J.T. Irvine, S. Tao, Ammonia and related chemicals as potential indirect hydrogen storage materials, *Int. J. Hydrog. Energy* 37 (2012) 1482-1494.
- [11] A. Valera-Medina, F. Amer-Hatem, A.K. Azad, I.C. Dedoussi, M.d. Joannon, R.X. Fernandes, P. Glarborg, H. Hashemi, X. He, S. Mashruk, J. McGowan, C. Mounaim-Rouselle, A. Ortiz-Prado, A. Ortiz-Valera, I. Rossetti, B. Shu, M. Yehia, H. Xiao, M. Costa, Review on Ammonia as a Potential Fuel From Synthesis to Economics, *Energy Fuels* 35 (2021) 6964–7029.
- [12] O. Mathieu, E.L. Petersen, Experimental and modeling study on the high-temperature oxidation of Ammonia and related NO_x chemistry, *Combust. Flame* 162 (2015) 554-570.
- [13] J.A. Miller, C.T. Bowman, Mechanism and modeling of nitrogen chemistry in combustion, *Prog. Energy Combust. Sci.* 15 (1989) 287-338.

- [14] O. Kurata, N. Iki, T. Inoue, T. Matsunuma, T. Tsujimura, H. Furutani, M. Kawano, K. Arai, E.C. Okafor, A. Hayakawa, H. Kobayashi, Development of a wide range-operable, rich-lean low-NO_x combustor for NH₃ fuel gas-turbine power generation, *Proc. Combust. Inst.* 37 (2019) 4587-4595.
- [15] A.M. Elbaz, S. Wang, T.F. Guiberti, W.L. Roberts, Review on the recent advances on ammonia combustion from the fundamentals to the applications, *Fuel Communications* 10 (2022) 100053.
- [16] O. Herbinet, P. Bartocci, A. Grinberg Dana, On the use of ammonia as a fuel – A perspective, *Fuel Communications* 11 (2022) 100064.
- [17] C. Lhuillier, P. Brequigny, F. Contino, C. Mounaïm-Rousselle, Experimental study on ammonia/hydrogen/air combustion in spark ignition engine conditions, *Fuel* 269 (2020) 117448.
- [18] Q. Zhang, M. Li, S. Shao, G. Li, Ammonia emissions of a natural gas engine at the stoichiometric operation with TWC, *Applied Thermal Engineering* 130 (2018) 1363-1372.
- [19] M. Pochet, I. Truedsson, F. Foucher, H. Jeanmart, F. Contino, Ammonia-Hydrogen Blends in Homogeneous-Charge Compression-Ignition Engine, *SAE Technical Paper Series No. 2017-24-0087*, 2017.
- [20] K. Ryu, G.E. Zacharakis-Jutz, S.-C. Kong, Effects of gaseous ammonia direct injection on performance characteristics of a spark-ignition engine, *Applied Energy* 116 (2014) 206-215.
- [21] K.D.K.A. Somarathne, S. Hatakeyama, A. Hayakawa, H. Kobayashi, Numerical study of a low emission gas turbine like combustor for turbulent ammonia/air premixed swirl flames with a secondary air injection at high pressure, *Int. J. Hydrog. Energy* 42 (2017) 27388-27399.
- [22] M. Alnajideen, H. Shi, W. Northrop, D. Emberson, S. Kane, P. Czyzewski, M. Alnaeli, S. Mashruk, K. Rouwenhorst, C. Yu, S. Eckart, A. Valera-Medina, Ammonia combustion and emissions in practical applications: a review, *Carbon Neutrality* 3 (2024).
- [23] K. Machaj, J. Kupecki, Z. Malecha, A.W. Morawski, M. Skrzypkiewicz, M. Stanclik, M. Chorowski, Ammonia as a potential marine fuel: A review, *Energy Strategy Reviews* 44 (2022) 100926.
- [24] A.G. Szanthoffer, M. Papp, T. Turányi, Identification of well-parameterised reaction steps in detailed combustion mechanisms – A case study of ammonia/air flames, *Fuel* 380 (2025) 132938.
- [25] M. Monge-Palacios, X. Zhang, N. Morlanes, H. Nakamura, G. Pezzella, S.M. Sarathy, Ammonia pyrolysis and oxidation chemistry, *Prog. Energy Combust. Sci.* 105 (2024) 101177.
- [26] S.A. Alturaifi, O. Mathieu, E.L. Petersen, An experimental and modeling study of ammonia pyrolysis, *Combust. Flame* 235 (2021) 111694.
- [27] M.R. Wright, *Introduction to chemical kinetics*, John Wiley & Sons, Ltd, England, 2005.
- [28] R.W. Carr, *Elements of chemical kinetics*, *Comprehensive chemical kinetics* 42 (2007) 43-99.

- [29] H.-H. Carstensen, A.M. Dean, Chapter 4 The Kinetics of Pressure-Dependent Reactions, *Modeling of Chemical Reactions* 2007, pp. 101-184.
- [30] J.I. Steinfeld, J.S. Francisco, W.L. Hase, *Chemical kinetics and dynamics*, NJ: Prentice Hall, Upper Saddle River, New Jersey 07458, 1999.
- [31] C.K. Law, *Combustion physics*, Cambridge university press, 2010.
- [32] J. Troe, Theory of thermal unimolecular reactions in the fall - off range. I. Strong collision rate constants, *Berichte der Bunsengesellschaft für physikalische Chemie* 87 (1983) 161-169.
- [33] Reaction Design: San Diego, ANSYS Chemkin theory manual 20.2, 2025.
- [34] M. Pelucchi, C. Cavallotti, A. Cuoci, T. Faravelli, A. Frassoldati, E. Ranzi, Detailed kinetics of substituted phenolic species in pyrolysis bio-oils, *React. Chem. Eng* 4 (2019) 490-506.
- [35] X. Han, M. Lubrano Lavadera, A.A. Konnov, An experimental and kinetic modeling study on the laminar burning velocity of $\text{NH}_3 + \text{N}_2\text{O} + \text{air}$ flames, *Combust. Flame* 228 (2021) 13-28.
- [36] V.A. Alekseev, N. Bystrov, A. Emelianov, A. Eremin, P. Yatsenko, A.A. Konnov, High-temperature oxidation of acetylene by N_2O at high Ar dilution conditions and in laminar premixed $\text{C}_2\text{H}_2 + \text{O}_2 + \text{N}_2$ flames, *Combust. Flame* 238 (2022) 111924.
- [37] A. Burcat, B. Ruscic, Third millenium ideal gas and condensed phase thermochemical database for combustion (with update from active thermochemical tables), Argonne National Lab.(ANL), Argonne, IL (United States), 2005.
- [38] A.W. Jasper, E. Kamarchik, J.A. Miller, S.J. Klippenstein, First-principles binary diffusion coefficients for H, $\text{H}(2)$, and four normal alkanes + $\text{N}(2)$, *J Chem Phys* 141 (2014) 124313.
- [39] A.W. Jasper, J.A. Miller, Lennard-Jones parameters for combustion and chemical kinetics modeling from full-dimensional intermolecular potentials, *Combust. Flame* 161 (2014) 101-110.
- [40] F.N. Egolfopoulos, N. Hansen, Y. Ju, K. Kohse-Höinghaus, C.K. Law, F. Qi, Advances and challenges in laminar flame experiments and implications for combustion chemistry, *Prog. Energy Combust. Sci.* 43 (2014) 36-67.
- [41] A.A. Konnov, A. Mohammad, V.R. Kishore, N.I. Kim, C. Prathap, S. Kumar, A comprehensive review of measurements and data analysis of laminar burning velocities for various fuel+air mixtures, *Prog. Energy Combust. Sci.* 68 (2018) 197-267.
- [42] E. Ranzi, A. Frassoldati, R. Grana, A. Cuoci, T. Faravelli, A.P. Kelley, C.K. Law, Hierarchical and comparative kinetic modeling of laminar flame speeds of hydrocarbon and oxygenated fuels, *Prog. Energy Combust. Sci.* 38 (2012) 468-501.
- [43] V.A. Alekseev, Laminar burning velocity of hydrogen and flame structure of related fuels for detailed kinetic model validation, Doctoral Thesis (compilation), Combustion Physics, Lunds universitet, 2015.
- [44] P.H. Joo, J. Gao, Z. Li, M. Aldén, Experimental apparatus with full optical access for combustion experiments with laminar flames from a single circular nozzle at elevated pressures, *Rev. Sci. Instrum.* 86 (2015) 035115.

- [45] A. A. Konnov, The temperature and pressure dependences of the laminar burning velocity: experiments and modelling. In Proceedings of the European Combustion Meeting (March 30-April 2, 2015, Budapest, Hungary).
- [46] V.A. Alekseev, M. Christensen, A.A. Konnov, The effect of temperature on the adiabatic burning velocities of diluted hydrogen flames: A kinetic study using an updated mechanism, *Combust. Flame* 162 (2015) 1884-1898.
- [47] R.E. Cornell, M.C. Barbet, J. Lee, M.P. Burke, NH₃ oxidation by NO₂ in a jet-stirred reactor: The effect of significant uncertainties in H₂NO kinetics, *Appl. Energy Combust. Sci.* 12 (2022) 100095.
- [48] M. Lubrano Lavadera, Combustion kinetic characteristics of smart energy carriers in model reactors, Doctoral Thesis, Università degli Studi di Napoli Federico II, 2017.
- [49] V.A. Alekseev, J.D. Naucler, M. Christensen, E.J.K. Nilsson, E.N. Volkov, L.P.H. de Goeij, A.A. Konnov, Experimental Uncertainties of the Heat Flux Method for Measuring Burning Velocities, *Combust. Sci. Technol.* 188 (2016) 853-894.
- [50] L.P.H. de Goeij, A. Van Maaren, R. Quax, Stabilization of adiabatic premixed laminar flames on a flat flame burner, *Combust. Sci. Technol.* 92 (1993) 201-207.
- [51] K.J. Bosschaart, L.P.H.d. Goeij, Detailed analysis of the heat flux method for measuring burning velocities, *Combust. Flame* 132 (2003) 170-180.
- [52] S. Wang, Z. Wang, A.M. Elbaz, X. Han, Y. He, M. Costa, A.A. Konnov, W.L. Roberts, Experimental study and kinetic analysis of the laminar burning velocity of NH₃/syngas/air, NH₃/CO/air and NH₃/H₂/air premixed flames at elevated pressures, *Combust. Flame* 221 (2020) 270-287.
- [53] C.J. Rallis, A.M. Garforth, The determination of laminar burning velocity, *Proc. Combust. Inst.* 6 (1980) 303-329.
- [54] K.J. Bosschaart, Analysis of the heat flux method for measuring burning velocities, Master thesis, Eindhoven University Press, 2002.
- [55] A.A. Konnov, I.V. Dyakov, Measurement of propagation speeds in adiabatic cellular premixed flames of CH₄+O₂+CO₂, *Experimental Thermal and Fluid Science* 29 (2005) 901-907.
- [56] M. Matalon, Flame dynamics, *Proc. Combust. Inst.* 32 (2009) 57-82.
- [57] B. Li, Y. He, Z. Li, A.A. Konnov, Measurements of NO concentration in NH₃-doped CH₄+air flames using saturated laser-induced fluorescence and probe sampling, *Combust. Flame* 160 (2013) 40-46.
- [58] X. Han, Z. Wang, M. Costa, Z. Sun, Y. He, K. Cen, Experimental and kinetic modeling study of laminar burning velocities of NH₃/air, NH₃/H₂/air, NH₃/CO/air and NH₃/CH₄/air premixed flames, *Combust. Flame* 206 (2019) 214-226.
- [59] H. Nakamura, M. Shindo, Effects of radiation heat loss on laminar premixed ammonia/air flames, *Proc. Combust. Inst.* 37 (2019) 1741-1748.
- [60] S.A. Alturaifi, O. Mathieu, E.L. Petersen, Shock-tube laser absorption measurements of N₂O time histories during ammonia oxidation, *Fuel Communications* 10 (2022) 100050.

- [61] R. Tang, Q. Xu, J. Pan, J. Gao, Z. Wang, H. Wei, G. Shu, An experimental and modeling study of ammonia oxidation in a jet stirred reactor, *Combust. Flame* 240 (2022) 112007.
- [62] M.V. Manna, P. Sabia, R. Ragucci, M. de Joannon, Oxidation and pyrolysis of ammonia mixtures in model reactors, *Fuel* 264 (2020) 116768.
- [63] K.N. Osipova, O.P. Korobeinichev, A.G. Shmakov, Chemical structure and laminar burning velocity of atmospheric pressure premixed ammonia/hydrogen flames, *Int. J. Hydrog. Energy* 46 (2021) 39942-39954.
- [64] K.N. Osipova, S.M. Sarathy, O.P. Korobeinichev, A.G. Shmakov, Chemical structure of premixed ammonia/hydrogen flames at elevated pressures, *Combust. Flame* 246 (2022) 112419.
- [65] P. Glarborg, H. Hashemi, S. Cheskis, A.W. Jasper, On the Rate Constant for $\text{NH}_2 + \text{HO}_2$ and Third-Body Collision Efficiencies for $\text{NH}_2 + \text{H} (+\text{M})$ and $\text{NH}_2 + \text{NH}_2 (+\text{M})$, *J. Phys. Chem. A* 125 (2021) 1505-1516.
- [66] D. Zhu, Z. Qu, M. Li, S. Agarwal, R. Fernandes, B. Shu, Investigation on the NO formation of ammonia oxidation in a shock tube applying tunable diode laser absorption spectroscopy, *Combust. Flame* 246 (2022) 112389.
- [67] A.A. Konnov, I.V. Dyakov, J.D. Ruyck, Nitric oxide formation in premixed flames of $\text{H}_2 + \text{CO} + \text{CO}_2$ and air, *Proc. Combust. Inst.* 29 (2002) 2171-2177.
- [68] N.L. Haworth, J.C. Mackie, G.B. Bacskay, An Ab Initio Quantum Chemical and Kinetic Study of the $\text{NNH} + \text{O}$ Reaction Potential Energy Surface : How Important Is This Route to NO in Combustion, *J. Phys. Chem. A* 107 (2003) 6792-6803.
- [69] S.J. Klippenstein, L.B. Harding, P. Glarborg, J.A. Miller, The role of NNH in NO formation and control, *Combust. Flame* 158 (2011) 774-789.
- [70] X. Han, Z. Wang, Y. He, Y. Zhu, K. Cen, Experimental and kinetic modeling study of laminar burning velocities of NH_3 /syngas/air premixed flames, *Combust. Flame* 213 (2020) 1-13.
- [71] X. Zhang, S.P. Moosakutty, R.P. Rajan, M. Younes, S.M. Sarathy, Combustion chemistry of ammonia/hydrogen mixtures: Jet-stirred reactor measurements and comprehensive kinetic modeling, *Combust. Flame* 234 (2021) 111653.
- [72] A. Stagni, C. Cavallotti, S. Arunthanayothin, Y. Song, O. Herbinet, F. Battin-Leclerc, T. Faravelli, An experimental, theoretical and kinetic-modeling study of the gas-phase oxidation of ammonia, *React. Chem. Eng* 5 (2020) 696-711.
- [73] A.G. Szanthoffer, I.G. Zsély, L. Kawka, M. Papp, T. Turányi, Testing of NH_3/H_2 and NH_3 /syngas combustion mechanisms using a large amount of experimental data, *Appl. Energy Combust. Sci.* 14 (2023) 100127.
- [74] P. Glarborg, E. Fabricius-Bjerre, T.K. Joensen, H. Hashemi, S.J. Klippenstein, An experimental, theoretical and kinetic modeling study of the $\text{N}_2\text{O}-\text{H}_2$ system: Implications for $\text{N}_2\text{O} + \text{H}$, *Combust. Flame* 271 (2025) 113810.
- [75] X. Han, Z. Wang, Y. He, Y. Liu, Y. Zhu, A.A. Konnov, The temperature dependence of the laminar burning velocity and superadiabatic flame temperature phenomenon for NH_3 /air flames, *Combust. Flame* 217 (2020) 314-320.

- [76] K.P. Shrestha, C. Lhuillier, A.A. Barbosa, P. Brequigny, F. Contino, C. Mounaïm-Rousselle, L. Seidel, F. Mauss, An experimental and modeling study of ammonia with enriched oxygen content and ammonia/hydrogen laminar flame speed at elevated pressure and temperature, *Proc. Combust. Inst.* 38 (2021) 2163-2174.
- [77] A. Hamadi, N. Obrecht, C. Callu, A. Stagni, T. Faravelli, A. Comandini, N. Chaumeix, Experimental and modeling investigation of the laminar flame speeds for ammonia with various oxygen and diluent mixtures, *Proc. Combust. Inst.* 40 (2024) 105387.
- [78] A.W. Jasper, Predicting third-body collision efficiencies for water and other polyatomic baths, *Faraday Discuss* 238 (2022) 68-86.
- [79] S.J. Klippenstein, C.R. Mulvihill, P. Glarborg, Theoretical Kinetics Predictions for Reactions on the NH_2O Potential Energy Surface, *J Phys Chem A* 127 (2023) 8650-8662.
- [80] J.A. Miller, M.D. Smooke, R.M. Green, R.J. Kee, Kinetic Modeling of the Oxidation of Ammonia in Flames, *Combust. Sci. Technol.* 34 (2007) 149-176.
- [81] R.A. Schwind, J.B. Sinrud, C.C. Fuller, M.S. Klassen, R.A. Walker, C.F. Goldsmith, Experimental study of linear burning rates of liquid nitromethane using a novel high-pressure continuous feed liquid strand burner, *Proc. Combust. Inst.* 39 (2023) 5083-5090.
- [82] E.S. Starkman, Nitroparaffins as potential engine fuel, *Industrial & Engineering Chemistry* 51 (1959) 1477-1480.
- [83] S. Raviteja, P.A. Ramakrishna, A. Ramesh, Laminar Burning Speeds of Nitromethane-Gasoline Blends at Elevated Temperatures and Pressures, *Journal of Energy Resources Technology* 141 (2019) 042202.
- [84] D. Zheng, D. He, Y. Du, Y. Ding, Z. Peng, Nitromethane as a nitric oxide precursor for studying high-temperature interactions between ammonia and nitric oxide in a shock tube, *Combust. Flame* 250 (2023) 112644.
- [85] O. Mathieu, B. Giri, A.R. Agard, T.N. Adams, J.D. Mertens, E.L. Petersen, Nitromethane ignition behind reflected shock waves: Experimental and numerical study, *Fuel* 182 (2016) 597-612.
- [86] K.P. Shrestha, L. Seidel, T. Zeuch, G. Moréac, P. Dagaut, F. Mauss, On the implications of nitromethane – NO_x chemistry interactions for combustion processes, *Fuel* 289 (2021) 119861.
- [87] P. Glarborg, A.B. Bendtsen, J.A. Miller, Nitromethane dissociation: Implications for the $\text{CH}_3 + \text{NO}_2$ reaction, *Int. J. Chem. Kinet.* 31 (1999) 591-602.

